Design Science

Improving the feel of 3D printed prototypes for new product development: A feasibility study of emulating mass properties by optimising infill structures and materials

Harry Felton [ID], Jason Yon and Ben Hicks

Department of Mechanical Engineering, University of Bristol, Bristol, UK

Abstract

Product prototypes and particularly those that are 3D printed will have mass properties that are significantly different from the product they represent. This affects both functional performance and stakeholder perception of the prototype. Within this work, computational emulation of mass properties for a primitive object (a cube) is considered, developing a baseline numerical method and parameter set with the aim of demonstrating the means of improving feel in 3D printed prototypes. The method is then applied and tuned for three case study products – a games controller, a hand drill and a laser pointer – demonstrating that product mass properties could be numerically emulated to within ~1% of the target values. This was achieved using typical material extrusion technology with no physical or process modification. It was observed that emulation accuracy is dependent on the relative offset of the centre of mass from the geometric centre. A sensitivity analysis is further undertaken to demonstrate that product-specific parameters can be beneficial. With tuning of these values, and with some neglect of practical limitations, emulation accuracy as high as ~99.8% can be achieved. This was shown to be a reduction in error of up to 99.6% relative to a conventional fabrication.

Keywords: Prototyping, Design methods, 3D Printing, Perception, Product development

1. Introduction

Prototypes are a critical part of the design process (Ullman 2010; Camburn *et al.* 2017), often considered crucial to the success of product development. They provide insight into how a product may look, function or otherwise exist (Houde & Hill 1997), and can be created in either the virtual or the physical domain or a combination thereof (Gibson, Gao & Campbell 2004). This is summarised by Houde & Hill (1997), who give one of the broadest definitions in literature, saying, "We define a prototype as any representation of a design idea – regardless of medium". As such, a prototype may take a wide variety of forms, and it is generally up to the designer to identify the prototyping objective and thereby

an appropriate prototype form. To do this, several aspects are considered, including the following:

- Purpose – What information should be developed through the prototyping activity?
- Design stage – How developed is the product?
- Fidelity (or precision) – How similar should the prototype be to the as-designed product?
- Construction – What resources are available for the fabrication of the prototype?

Several authors have highlighted the importance of understanding the purpose of a prototype. For example, Houde and Hill (1997) define four primary purposes: "Look and Feel", "Role", "Implementation" and "Integrated" prototypes. Each of these matches very similarly to the categories proposed by Buchenau and Suri (2000) – looks-like, behaves-like and works-like, respectively, with integrated prototypes being a combination of these. Of note is the lack of reference to the "feel" of the prototype in the latter work (Buchenau & Suri 2000). This is in contrast to Houde and Hill and several others, including Ulrich & Eppinger (2016), who consider the physicality of prototypes as a key factor (Ulrich & Eppinger 2016). This said, there is argument for "behaves-like" prototypes to consider part of the feel of a prototype, with this being a broad term covering aspects such as surface finish, mass properties, materials, temperature in operation and ergonomics.

Similarly, the stage of design is considered in literature and regarded as an important constraint on prototypes heavily influencing the type of prototype that should be produced (Ullman 2010). In accord, this impacts the level of fidelity of the prototype – that is how closely the prototype should match the designed product – and which heavily impacts how the prototype is perceived (Sauer & Sonderegger 2009; Lauff, Kotys-Schwartz & Rentschler 2017; Mathias *et al.* 2019). High-fidelity prototypes are those that represent the aspects previously discussed to a higher degree (e.g., more representative looks, feel, behaviour and implementation).

To achieve the desired prototype, it must be constructed, either virtually or physically. Although there are benefits to prototypes developed in each of the physical and virtual domains, it is generally accepted that physical prototypes offer a tangibility that cannot be (currently) achieved using virtual prototypes (Wiethoff *et al.* 2013; Hamon *et al.* 2014; Donati & Vignoli 2015). Other aspects, including visual aspects and functional analysis can be achieved more readily in the virtual domain. As such, tangible aspects of design are likely to be the focus of many physical prototypes, which allow users to understand a product's "feel" (Deininger *et al.* 2019).

Physical prototypes can be made in many ways. Appropriate fabrication methods range from cardboard and junk modelling, to advanced computer-controlled machining – and several others in-between (Hallgrimsson 2012; Mathias *et al.* 2018). Each of these has its own advantages and disadvantages which must be considered by a designer when choosing their prototyping strategy. For example, junk modelling can provide a low-fidelity or low-detail understanding of what a product may look like at relatively low cost and time investment, whilst computer-controlled machining can give a much higher detail and fidelity of understanding but at much greater cost.

In industry, one notable example (amongst many) of prototype use and development is that of Dyson, who use a range of prototype fabrication methods. In one example, a vacuum cleaner prototype was developed using prototypes initially made from cardboard and junk, through advanced manufacture of plastic and internal components for testing (Felton, Yon & Hicks 2020). Notably, more recent prototypes have started to incorporate additively manufactured components.

Additive Manufacturing (AM) reduces the effort required to move from the virtual to the physical domain (Gibson *et al.* 2004), with available effort a common source of tension in design processes (Goudswaard *et al.* 2022). Although AM is beginning to be used for small-to-medium scale production, the majority of its use (>50%) is in 3D printing during the early stages of product development (Sculpteo 2021), where over 70% of designers have access to in-house Material Extrusion (MEX) facilities. The use of the technology for prototyping is wide-spread in literature (Bassoli *et al.* 2012; Manoharan *et al.* 2013). Given their prevalence, the focus of this research is on thermoplastic-based MEX technology.

The fabrication time for a part produced via the MEX process is principally dependent upon the deposition rate and volume of deposited material. Although other factors such as deposition head travel also have an effect, this is generally smaller. To reduce process time, low-infill-density patterns are encouraged – typically 10% to 30% (Luzanin *et al.* 2017). For large print volumes this can significantly reduce fabrication time, material costs and energy but at the expense of mechanical and functional properties. As a consequence, the effect of infill density has been extensively researched. This includes the impact on mechanical properties (Lanzotti *et al.* 2015; Melenka *et al.* 2015; Villacres, Nobes & Ayranci 2018; Goudswaard, Hicks & Nassehi 2020; Schmitt, Mehta & Kim 2020) and optimisation for given applications (such as automotive (Schmitt *et al.* 2020)). To date, the targeting of specific mass properties in MEX fabrication (including through changing the infill density) has had little attention outside of minimising infill for mass reduction.

It is generally accepted that mass properties – mass, balance and rotational inertia (RI) – influence a user's perception of a prototype (Felton *et al.* 2020), affecting the "feels-like" nature of prototypes. Further, it has been shown that a user's performance changes depending upon the mass properties of the equipment used (e.g. in sport (Mitchell, Jones & King 2000; Nathan 2003; Cross & Bower 2006). As such, if a product prototype is created for the purpose of user interaction, an accurate representation of mass properties must be considered. However, the authors have not been able to identify any work that looks at promoting the fabrication of prototypes with representative mass properties using otherwise low-fidelity models. This is problematic, as many of these models are able to take an accurate form, thus leading to inconsistencies in how a product may feel during user interaction – that is looks like but does not feel like when interacted with. This is particularly true for MEX parts, which generally feature very good geometric accuracy but poor mass property representation. Three primary factors affect the representation of product mass properties within an MEX prototype:

1. The use of low-density infill to speed up fabrication, which heavily influences overall mass but is rarely the reason a particular infill density is selected. Additionally, current infill design methods do not consider the distribution

of mass through a product, with most approximating to a near-homogenous structure.

2. The use of thermoplastics (which are still dominant in most sectors), such as PLA, ABS or PETG, rather than the intended material. This is principally because thermoplastic fabrication is much cheaper but comes at the penalty of the *feel* because the "as-designed" material is not used. For example, the material density, thermal conductivity and hardness discrepancies (amongst others) between steel and PLA will cause a user to perceive these differently. For the remainder of this article the authors use "as-designed" to denote the current embodiment of a design and its properties if it were manufactured.

3. The absence of internal components and/or geometry means that the internal structure's mass distribution is unrepresentative of the as-designed product. Simplification of internal geometry is often performed, especially in early-stage prototyping where the information about the prototype may be incomplete or abstract.

The authors note that many other machine and process factors (Afonso *et al.* 2021) will affect the precision and repeatability of mass property representation. However, many of these can be mitigated through careful control of the MEX process and/or software parameter adjustments. Further, their effect is second or third order compared to the as-designed versus 3D printed mass properties.

2. Research contribution

Given the importance of mass properties for consumer products and the prevalence of MEX for prototyping, it can be asserted that methods to improve mass property representation within MEX prototypes are needed. This would allow higher fidelity prototypes to be fabricated more readily in earlier design stages with minimal additional resource required. Through doing so, the design process can be accelerated through identification of issues related to the feel from mass properties earlier, and at a time of lower sunken cost.

This article presents the development of a numerical methodology for emulation (herein used to refer to imitation) of the as-designed mass properties of consumer products in MEX prototypes. It is recognised, however, that the effect on the user should be minimised to ensure MEX retains its advantages as a prototype fabrication method. As such, control of the infill composition – referring to the infill structure and deposition material – is investigated. This, along with the development methodology, process outline and results, is discussed throughout the rest of this article. The overall contribution aims to be a method through which a user may numerically emulate a product's mass properties ready for physical fabrication through MEX. This would be a first-of-its-kind approach.

3. An objective function for emulating mass properties

Emulating mass properties is not as straightforward as matching overall mass. Rather, mass properties, including overall mass, balance and RI, must be emulated and the relative importance may not be equal. It is therefore necessary to consider all these aspects in the development of the objective function for mass property emulation. Previous work has evaluated and discussed this (Mitchell

et al. 2000; Nathan 2003; Cross & Bower 2006; Felton *et al.* 2020), demonstrating the following:

1. Principal RI can generally be neglected, with other factors dominating the perceived RI of a product (Felton 2022).
2. Mass and mass balance are both perceived by users and should be considered.

Given these findings and the types of case considered (consumer artefacts), RI was not included in the objective function. The objective function was instead formed such that it considered mass and mass balance – taken as the Centre of Mass (CoM) position – alone. As such, the objective function can be defined as follows:

$$Obj.Function = am + bC_x + dC_y + eC_z$$

Equation 1 – *Objective Function definition. M is the mass error and C the error in each respective axis.*

Where a, b, d and *e* are set such that the mass property terms can be considered normalised. Correspondingly, a 1% change in mass is equivalent to a 1% error in the CoM position in each axis relative to the product's dimension along the axis. The applicability of this weighting may differ based on the use case but was considered appropriate for the development and demonstration of capability.

4. Methodology development

As previously stated, control of the infill composition provides the basis for mass emulation. The feasibility of this approach was verified via some simple mass calculations for a range of consumer goods. This demonstrated that the mass of these products could be achieved through the deposition of commercially available filaments. In addition, the increasing availability of multi-material printers allows for the deposition of two or more materials with distinctly different densities, allowing greater control over mass properties (distribution). Hence, minimal additional input from the designer and/or modification of the fabrication process would be required. This ensures the hypothetical ease of use and accessibility of the method.

The emulation methodology was intended to fit between the current design (e.g. CAD) and "slice" processes within the MEX pre-process workflow. This meant that virtual representations of form were available, though the method of definition may be variable. To overcome this, the method used Ansys Mechanical to generate a finite volume mesh that defined the product's geometry. CHEXA elements were used due to their relative uniformity whilst, through small manipulations, ensuring smoother geometric representation than would be available with a similarly sized voxel mesh. Mesh quality was verified within the Ansys software. For the purposes of this work, it was not thought necessary to blend CHEXA elements with alternative formats (for example, CPENTA, CTETRA) that allowed for a more geometrically accurate shell definition. This was primarily because the inaccuracies in shell definition would result in only small volume discrepancies averaged over the part. Future work may investigate how the shell – which should remain a solid surface – can be more robustly modelled for the purposes of physical fabrication. This may include considering the shell separately from the infill (with
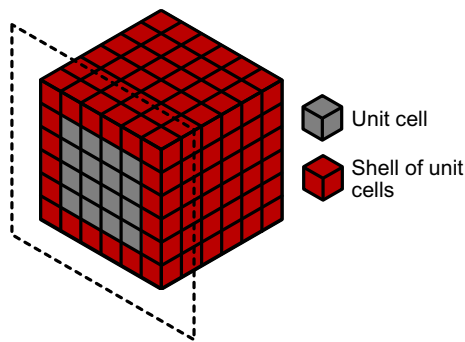
Figure 1. Example definition of part in unit cells, cut-through to show that the shell is formed of a single layer of unit cells.

the mass effect of the shell considered as a constant). For this work a unit cell width, solid shell was identified and used for simplicity, shown in Figure 1.

The finite volume mesh was then fed into bespoke code written in Python 3.8 (Python Software Foundation 2019), with open-source dependencies Numpy (Harris *et al.* 2020) and SciPy (Virtanen *et al.* 2020). This code carried out a directed optimisation approach which leveraged solution space knowledge. Local and global optimisation methods were tested, but inefficiencies caused by local minima, the large number of cells and the central limit theorem meant that these methods were unfeasible without modification. The result from the directed approach (see Section 4.1) generated an infill composition with a cellwise density – and therefore deposition – definition. To get to this stage, factors affecting the manufacturability and numerical performance of the emulation were considered.

The first consideration was whether continuous or discrete cellwise infill densities were used. It was decided that discrete density options should be used for two reasons. The first was that generating a support structure within the infill – to provide confidence that all layers were adequately supported – would be easier with a consistent minimum deposition. The second considered the numerical performance associated with each option; with which it can be demonstrated that two discrete results at opposite ends of a range will provide a more diverse set of results than a continuous distribution. For this reason, the terms high-density cell and low-density cell are used. In these instances, a high-density cell refers to mesh cells that have had the increased infill density (solid) and, where applicable, increased material density applied to them. Conversely, a low-density cell is that which is selected to use the base material (PLA in all instances) and the minimum viable infill structure (discussed in greater depth in Section 4.3).

The directed optimisation method (outlined in Section 4.1) using this basis was evaluated using an i5 9600-based desktop computer and an M1 MacBook Pro. These processors were thought representative of most mid- to high-end computers available on the market in 2020/21. Target runtimes were set to between 2 and 3 minutes to limit disruption to user workflow.

For initial development, a 50 mm cube was used with a target mass of 125 g and CoM position offset from the Geometric Centre (GC) of +2.5 mm in each axis. This is herein referred to as the development case. It is recognised that the use of a

regular primitive may lead to certain relationships being affected by the unique uniformity of the mesh and mass properties. While this may limit extrapolation of results to a non-uniform mesh, advantages of this approach include the ability to observe limitations associated with the use of primitive geometry, and to allow for deeper understanding of the causes of errors. Where appropriate, issues associated with the use of a cube for development are highlighted. Further mitigation is performed via a sensitivity analysis reported in Section 5.5.

To ensure the process provides acceptable accuracy in mass property emulation, investigation and characterisation of several important factors were performed. Relevant controlling factors include optimisation method, infill density and pattern, print materials, internal structure, cell size and the number of method repetitions. These are each discussed in Sections 4.1 through 4.5, respectively.

4.1. Directed optimisation method

The directed optimisation approach employed – based on solution space knowledge – uses a probability distribution across the mesh body, biased by the target CoM position. A flowchart of this process is given in Figure 2, and the original code is available via doi:10.5281/zenodo.8128282 https://zenodo.org/badge/latestdoi/664349403. Figure 3 also presents the method graphically, breaking each step down and demonstrating what is happening within the code. Initially, the method finds the shell's GC and desired CoM position (the position of the CoM of the as-designed product or a position being investigated as part of the design process), Figure 3. By using the mass and CoM offset from the GC, a target CoM for the internal volume can be calculated, Figure 3b. This is based on balancing mass moments around the desired CoM. A probability distribution – in this work an exponential probability distribution – is then applied around the internal volume target CoM position, Figure 3c, with the controlling parameters set by the required internal volume mass. This provides each cell with a probability of having a high density (instead of the minimum infill structure). Several iterations are then carried out using this probability function, with each cell's density calculated using Monte Carlo analysis, Figure 3d. From here, the actual mass of the internal volume and CoM can be averaged, in turn allowing the part's CoM to be calculated, Figure 3e. Depending on the exit conditions, the process can then finish or iterate by updating the CoM target position of the internal volume, Figure 3f. If the process exits, many more iterations of the internal cell structure are generated using Monte Carlo analysis to find the final result.

For a user, the application of this method should have little effect on the pre-process workflow. The only additional, manual steps for the user are to do the following:

1. Define the targeted mass properties; and,
2. Generate a finite volume mesh.

It may be possible for both steps to be integrated into a single toolchain with extended development (of the tool and AM file formats that may contain product data).

4.1.1. Internal volume centre of mass searching

To find the target CoM position, iterative searching was used. This had three independent exit conditions, any one of which would cause the method to move to

7/34
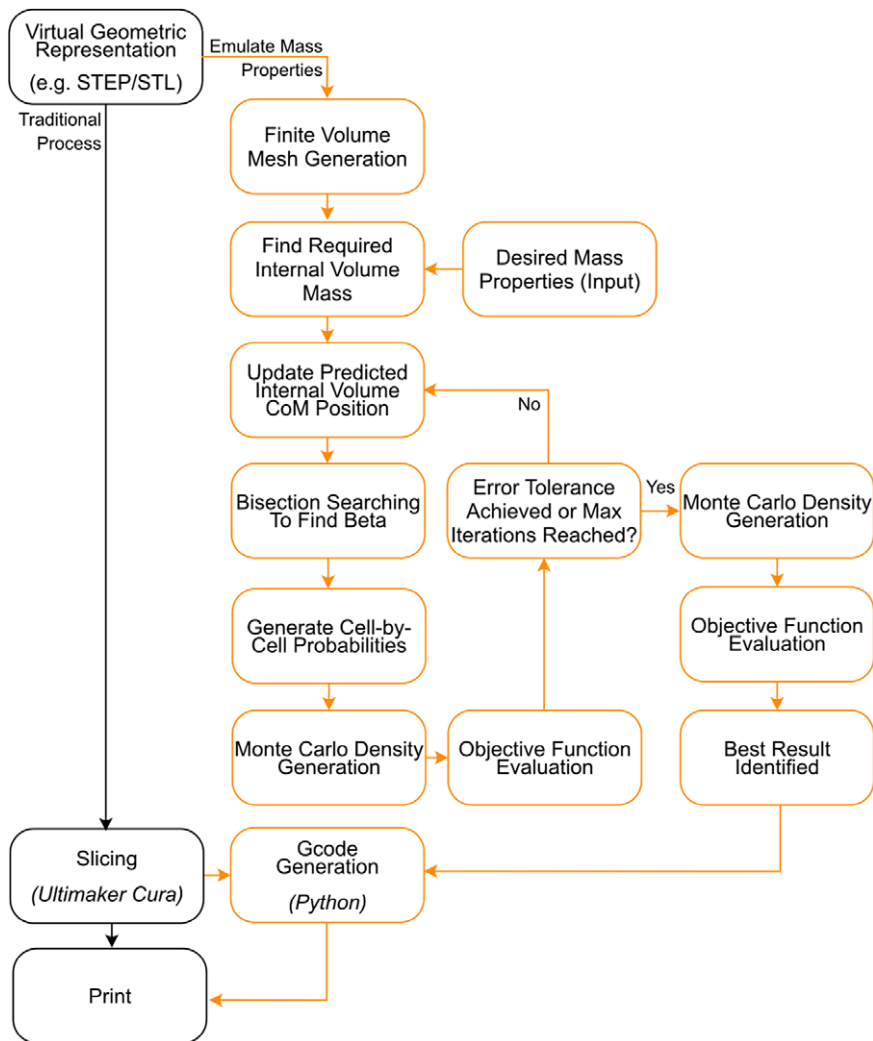
Figure 2. Flowchart outlining the directed optimisation approach.

the next processing stage. These were when the overall tolerance was met, the maximum number of iterations was reached and/or the error between iterations was within an allowable range.

For simulations where the maximum number of iterations was met, the number of iterations allowable was directly proportional to the runtime. This can be seen on the right-hand axis of Figure 4, with each iteration taking roughly 13.5 seconds. Model accuracy is also proportional to the maximum number of iterations. A balance is thus required between result accuracy and runtime. For this study, a maximum number of 8 iterations was set, with the allowable error (both absolute and between iterations) set to 0 such that development runs were aiming for the best result possible.

For each iteration, the CoM was estimated through the generation of cellwise probabilities to determine each cell mass. Due to the stochastic nature of this
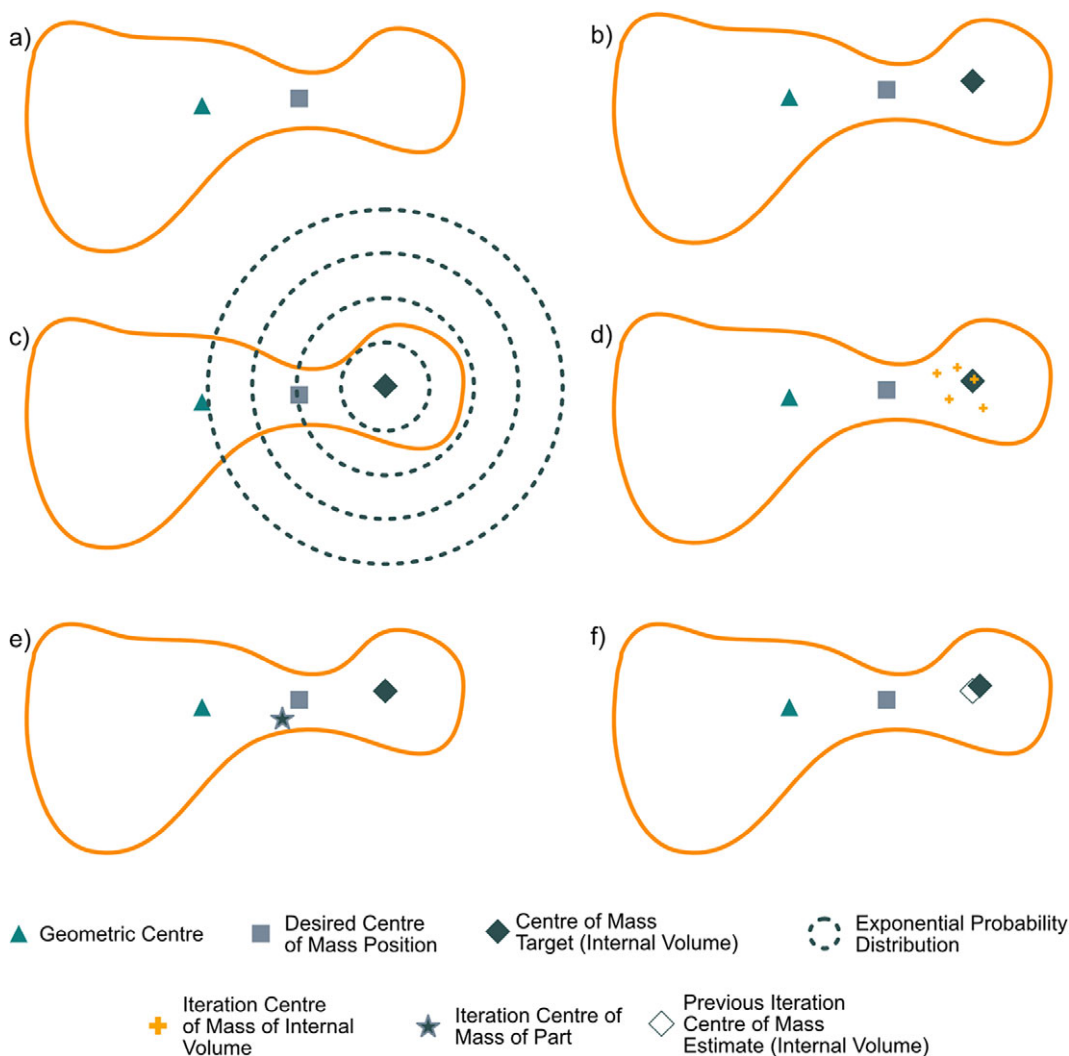
Figure 3. Directed optimisation methodology, broken down by step, to show the code function, in two dimensions. (a) The desired centre of mass position and geometric centre are identified. (b) The target centre of mass, to balance the geometric centre and provide the desired centre of mass position, is identified. (c) A probability distribution is formed around the target centre of mass position, providing each cell with a probability of having a higher density. (d) Several iterations of cell distributions (based on the prior probability distributions) are considered, and the actual centre of masses calculated. (e) The part level centre of mass position is found for the given iteration. (f) If the calculated iteration centre of mass for the part is out of acceptable limits, the target centre of mass is updated, and the process iterates from step (c).

process, assessments are completed and averaged to find an internal volume CoM for the given target and probability distribution shape parameter (β). To ensure consistency in estimations, the CoM iterations limit was set to 5 (derived from data presented in Figure 5 that presents process accuracy for various numbers of iterations).

4.1.2. Beta (β) tolerance

The probability distribution applied to the internal volume was chosen to be exponential (the shape controlled by shape parameter β). This distribution was chosen such that significant bias could be assigned to cells close to the target CoM when generating cellwise densities.

Using the scipy "minimize_scalar" bounded (Brent) method, the solution space is explored and returns a value for β that provides a suitable approximation for the number of high-density cells within the internal volume (relative to the required number). The smaller the allowable difference between the actual number and required number of higher-density cells – herein referred to as the β tolerance – the longer the runtime. As such, a value was sought to provide a balance between emulation accuracy and runtime. To investigate this, a range of β tolerances was investigated (Figure 6), which confirmed the relationship between runtime and β tolerance.

Overall, it can be asserted that increasing the β tolerance increases the objective function value. However, Figure 6 also demonstrates the relationship is inconsistent.

Prior to considering these behaviours, the application of the probability function should be understood. The function provides probability values for a continuous distribution of inputs with no limit. As a cell can be any distance from the target CoM (the input), a continuous probability distribution is required. However, the process uses a discrete mesh which, although dependent on the intricacy of product form, results in a high level of uniformity. As such, cells can be affected by the exponential distribution in clusters, depending on the target CoM position and β tolerance value used.

It is possible for the optimisation method to return a β value that is associated with a smaller difference than the stated maximum tolerance. It is contended that this was the cause of the large increases in objective function value between 5 and 11 and 12 and 14, and reduction after 25 (c.f. Figure 6). This is because, in conjunction with the effect of the discrete mesh above, it was possible for clusters of cells to be simultaneously affected by a small change in β. Additionally, due to the uniformity of the mesh that defines the cube, this effect may be exaggerated – especially in the case of a target CoM with consistent offsets in each axis.

The use of lower β tolerances – here observably less than 5 – reduced the overall objective function value consistently. As such, for the remainder of this work, a β tolerance of 4 is used as the best compromise between runtime and process accuracy.

It should be noted that the work here used a range of β values between 1 and 1000. For niche applications – particularly those where the internal CoM requires a large relative offset from the GC – the upper bound may need to be increased. It may be possible to achieve runtime improvements by changing the bounds, though this has not been considered within this work.

4.2. Materials

The most widely used material for MEX fabrication is PLA and as such has become the de facto standard for quality, cost, processing and availability. Consequently, PLA is used herein as the primary material. Work was completed to understand how changing the density of the secondary print material affected the results. To do
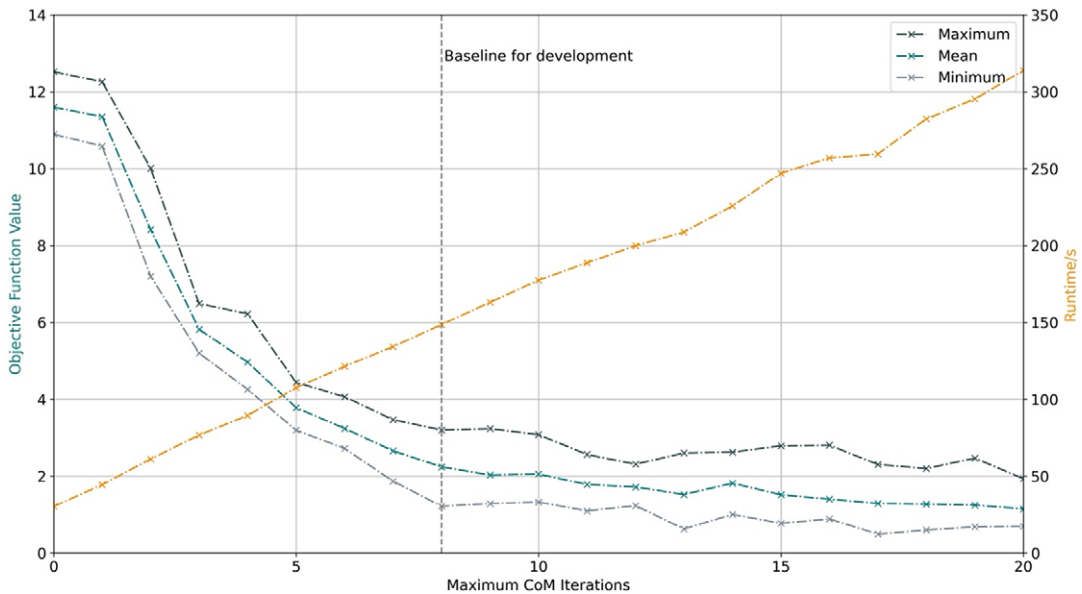
Figure 4. Effect of changing the maximum number of CoM search iterations on runtime and objective function value.

this, the term material density ratio (MDR) was defined, which was the ratio of the secondary print material density relative to the primary print material density (that is that of PLA).

MDRs between 1 and 9 times that of PLA were considered as this represented the extremes, i.e., lead. MDRs of less than 1 were considered out of scope of this work, though there may be real-world examples that require this. Extension to include these should be possible if appropriate materials are available. The results of this study are shown in Figure 7.

Figure 7 shows that for MDRs up to ~2.75, the CoM components (averaged) dominate the mass result. This is to be expected as mass cannot be localised as effectively with lower-density materials. The mass target can still be met as the total volume available is large enough to contain the required mass.

A consistent, minimum cost is reached at an MDR of ~3. At this point a compromise is reached where the maximum cell density is sufficient to move the CoM close to the target point whilst retaining a large enough number of high-density cells to precisely control the CoM position. For MDR values above this, the variability in mass increases significantly. It was thought this was because each high-density cell now had a relative greater effect on the mass property of the product. The issues associated with this are two-fold; firstly, the precision with which the product mass and CoM position can be controlled is reduced, and secondly, the stochastic nature of the method means that a change in a small number of cells has a greater impact on the result. As such, it was contended that an MDR between ~2.5 and 4 would be most advantageous for the method.

For the remainder of this article, copper-infused PLA is used as the secondary material. This material has an MDR of 2.75 (RS Components 2021), close to the aforementioned optimum. Testing was completed to ensure the materials could be
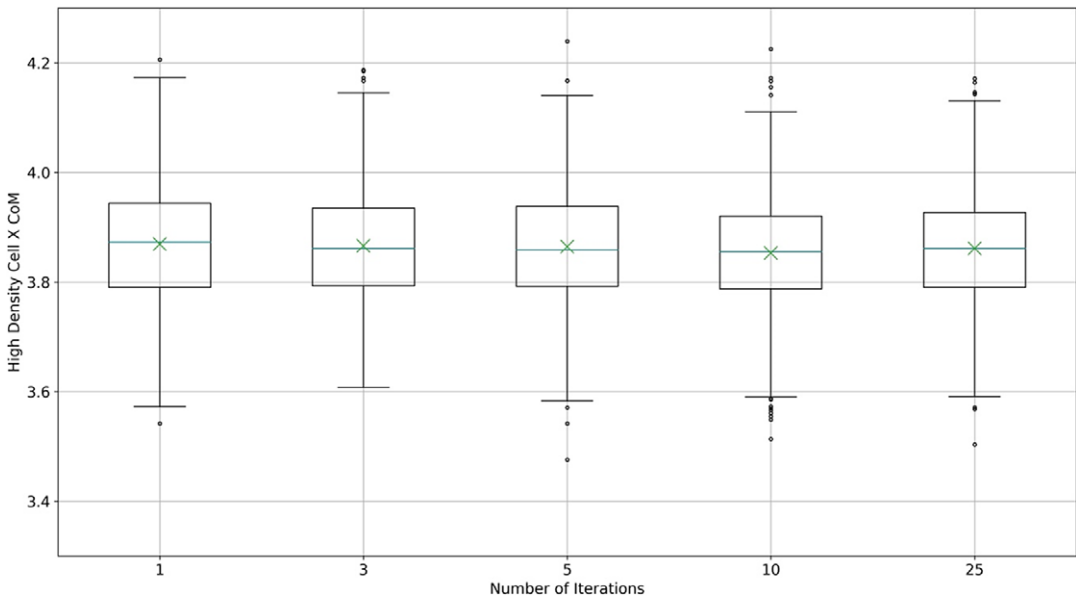
Figure 5. CoM variability vs number of iterations for given beta. The box represents the interquartile range (IQR), with the inside line the median. The whiskers represent 1.5 times the IQR, with the outliers marked. The mean is shown as an "x".

reliably printed together, with no issues observed. To reliably print metal-infused filaments such as this, a hardened nozzle would be required. This was not thought to be a significant limitation, with many first- and third-party hardened nozzles available for printers such as the Prusa i3 and Ultimaker 3.

4.3. Internal structure

To allow volumes of higher-density material to be printed, a supporting infill structure was needed. Although this could simply be reduced to a homogenous percentage infill density and pattern, available in most slicers already, this approach gives rise to three potential issues:

1. the infill pattern may not be evenly distributed throughout the cells;
2. the infill density may need to be large to provide sufficient support to every cell, especially when using small cells; and,
3. print path planning complexity would increase when slicing, with the starting point for a high-density cell, as well as the print directions, differing for each cell depending on where the support is located.

To overcome the issues associated with using a homogenous infill pattern, a cell-based infill structure – where every cell has a consistent minimum structure – was investigated.

Before considering various support structures, the effect of relative minimum cell density on objective function value was investigated. This is illustrated in Figure 8, with objective function value increasing with increasing minimum relative cell density. It should be noted that the relative minimum cell density was assumed to be directly related to the relative maximum cell density, as the
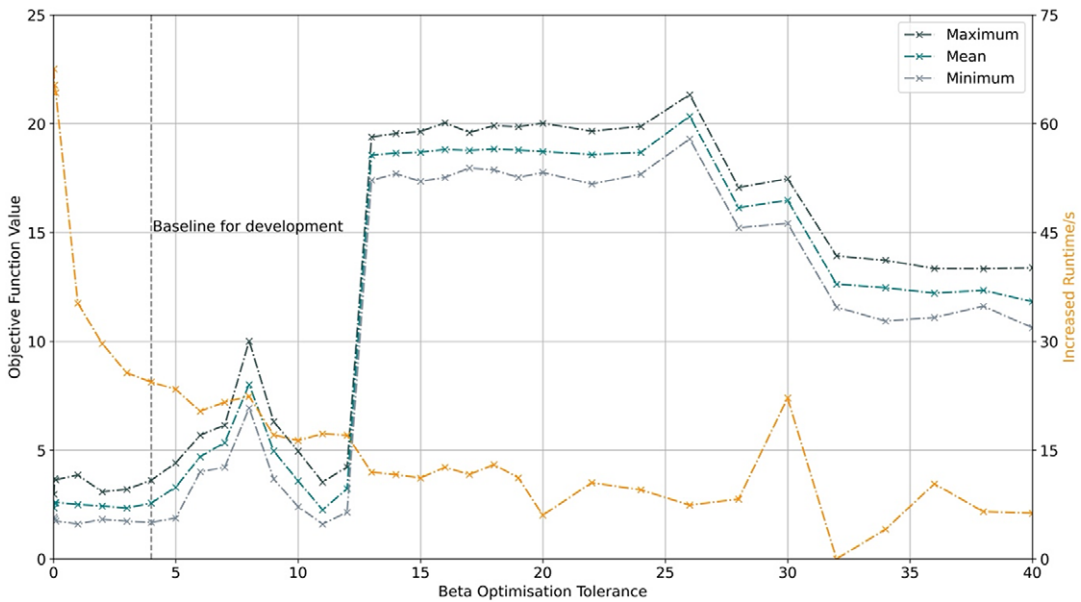
Figure 6. β tolerance against objective function value and runtime.

high-density cell structure would be printed around the minimum structure. This was done to improve theoretical print times, slicing process efficiency and print quality by using a single material for the base structure.

As the proportion of product volume that must be filled with PLA increases, the minimum mass must increase. Further, as the higher-density material can no longer fill as much of the product volume, the maximum mass must decrease. Therefore, the achievable mass envelope of the method decreases with increasing relative minimum cell density. CoM position is similarly affected. The main cause of this is the increased effective mass at the GC of the product. Additionally, the difference between the maximum and minimum cell mass reduces, further increasing the number of high-density cells required. As such, the objective function value increases. The variability between Monte Carlo optimisation (MCO) iterations, for both mass and CoM position, would lessen due to the reduced effect of individual cells.

The design of the internal structure was therefore an important consideration to ensure that the minimum material could be deposited per cell whilst ensuring sufficient support was provided. Several infill designs were considered – presented in Figure 9c. Each of the proposed structures was intended to provide varying levels of support that were proportional to the volume of material deposited whilst trying to minimise the volume of support structure that was used.

The absolute support provided, and material volume, was dependent upon cell and nozzle sizes. For this work, the cells were assumed to be perfect cubes with two faces aligned to the z-axis, and the nozzle size assumed to be 0.4 mm. Slicer and print settings were otherwise left as the default from Ultimaker Cura. Figure 9a shows the change in minimum relative cell density for each infill structure and varying cell sizes. The single-edge design – where a single track of material running along a cell's edge is shared by the adjoining cells – was the most appropriate for

13/34
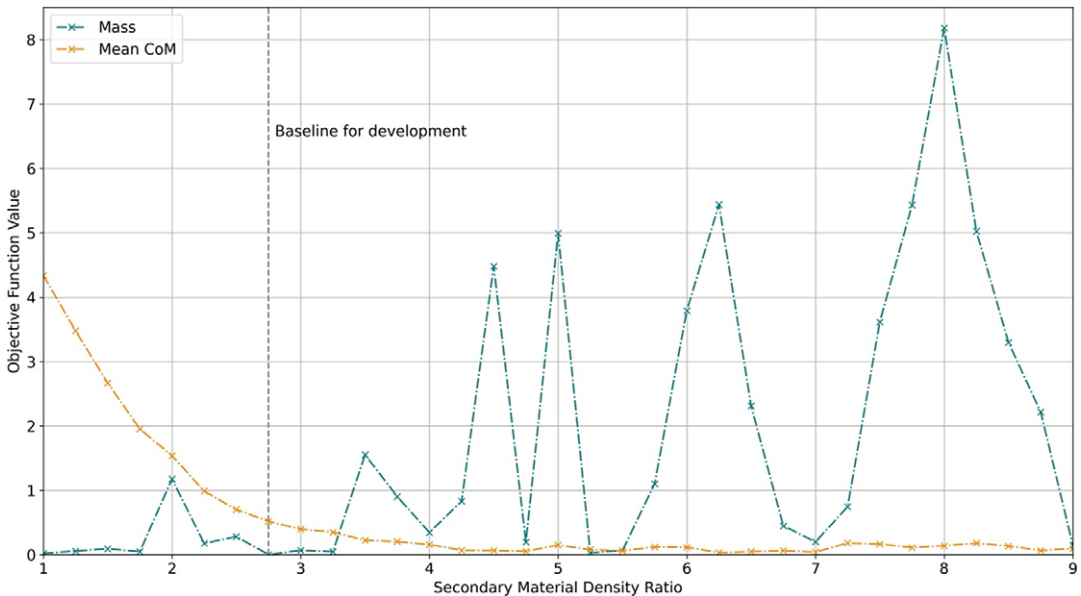
Figure 7. Objective function value, broken down into the mass component and average CoM component, for a range of material combinations. The secondary material density ratio is relative to PLA.

minimising the relative minimum cell density. However, it was recognised that it was also the most challenging with regards to reliably printing the solid cells due to each cell having the least support.

To understand how each infill structure would support the high-density cells, several test pieces were printed for a range of cell sizes (1, 2, 3 mm – referring to their length in each of the orthogonal axes). The test pieces featured a minimal example of the PLA deposition of the support structure with a singular and two adjacent high-density cells. This structure assumed the use of cubic cells as would be the target output from the mesh. Images of each of these prints are shown in Figure 9b. The fabrication process demonstrated that the first unsupported layer dropped by up to ~1 cell size before recovering the remaining layers for all designs. This is equivalent to ~0.002 g of incorrectly deposited material – with the effect reduced when adjacent high-density cells were printed along the z-axis. As such, the shared single-edge design was used.

Although using the shared-edge infill design would not ensure that mass distribution was kept consistent for each cell (due to inconsistent cell edges having material deposited), the distribution was consistent when considering two cells together, averaging out over the internal volume. Additionally, the mass contained in each of the low-density cells was thought small enough that the effect on result accuracy was negligible.

4.4. Cell size

Cell size inherently affects result accuracy and runtime. To investigate and quantify this effect, the emulation method was applied to a range of mesh densities for the
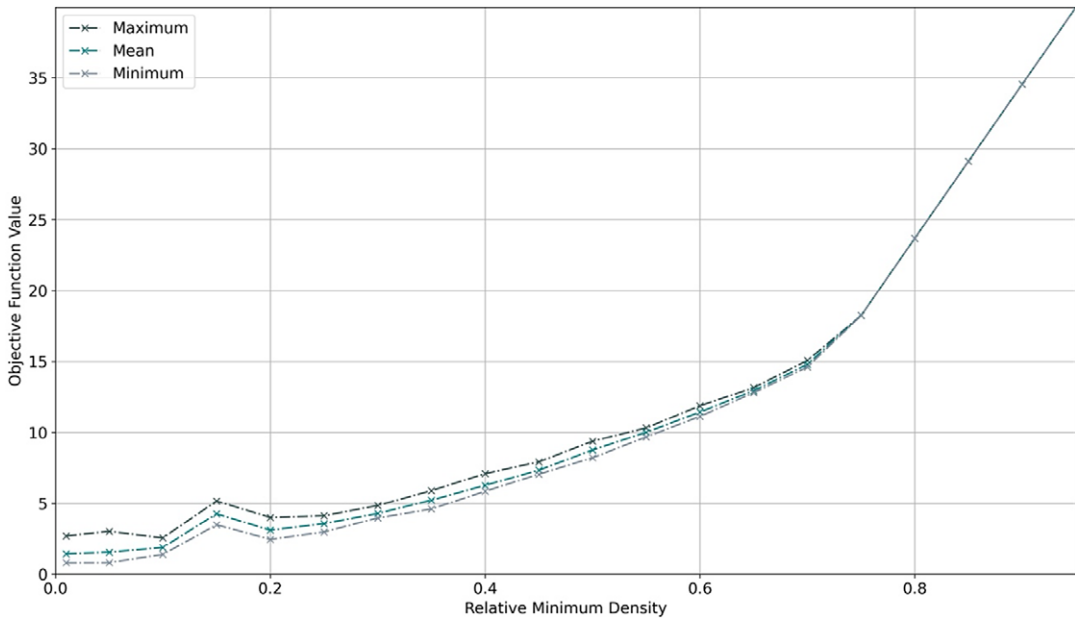
Figure 8. The effect of changing relative minimum density on objective function value.

development case. These results are presented in Figure 10. The figure demonstrates that the emulation result reaches an optimum when using the mesh with 2 mm cells. To explain this, two effects must be understood; the increased variability of the process when using larger cells (as each cell affects the calculation more significantly) and the increase in relative minimum cell density when using smaller cells. As such, a compromise is required. Process runtime must also be considered, with a cubic relationship between the cell size and process runtime. Although a time saving could be found in using smaller cells (due to the reduction in the required number of MCO iterations), the required extra computation in the remainder of the code outweighs this effect. It is therefore advantageous to use larger cells for process efficiency.

For process baseline verification and validation, a mesh density of ~1.4 mm was used as this provided an acceptable runtime (2 to 3 minutes) and consistent, accurate results. This translated to ~46,600 cells. Based on this work, it may have been suitable to increase the cell size used to ~2 mm to slightly improve the emulation result and runtime. However, the improvement in variability was considered preferable for development purposes. For future applications of the process, it is recommended that cell sizes of between 1.2 and 2 mm are used, depending on the part scale, nozzle size, material combinations and available computational resource/runtime.

4.5. Monte Carlo optimisation

In general, completing a greater number of MCO iterations improves the result whilst increasing runtime. The results presented in Figure 11 used 10,000 samples for various numbers of iterations, from an overall sample of 50,000 results. Using
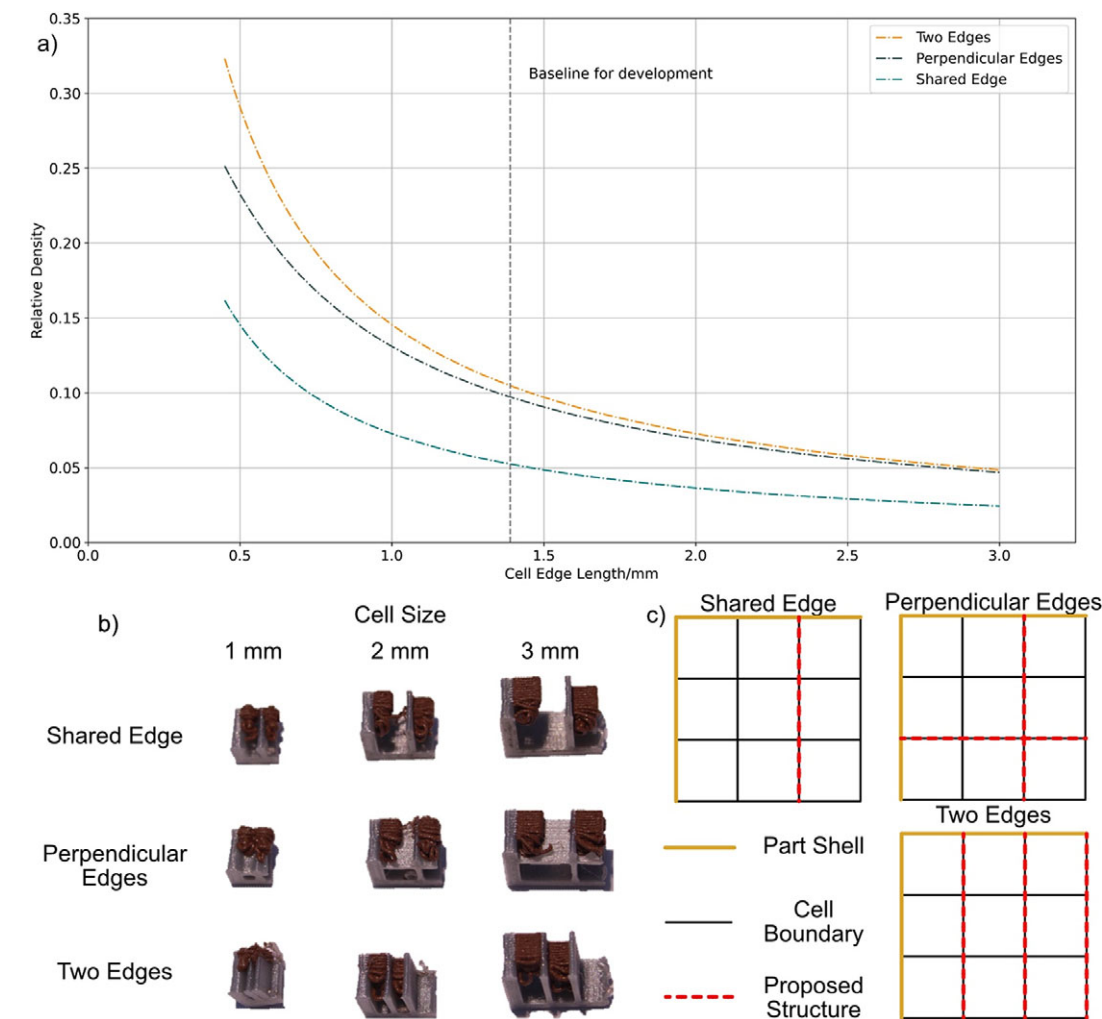
Figure 9. (a) Relative minimum density for the proposed infill structure designs, (b) Test prints showing the effect on overhangs when using the proposed infill structures for different cell sizes (printed with PLA and copper-infused PLA) (c) Investigated infill structures to achieve minimum deposition volume and required support.

this figure, it is possible to demonstrate that the median result – and total range of results – decreases with increasing MCO iterations. It can also be seen that the interquartile range of the results for 10, 25, 50 or 100 iterations is relatively consistent (between 0.31 and 0.44).

For the development of the method, 25 iterations were used in the MCO. This was applied to allow more data points to be investigated for the same computational time when compared to running a larger number of MCO iterations. As the aim of this study is to establish trends rather than absolute result values, this was deemed suitable. For final product emulation results, a larger number of iterations may be appropriate depending on the time available and the required accuracy of result.

5. Case studies

This section applies the methodology to three case study products (A to C). The results are first compared to those obtained via a conventional fabrication process, prior to conducting a sensitivity analysis aimed at tuning the method for each case.

5.1. Prototypical consumer products

The products selected are high-volume handheld devices that require high levels of human motor control for interaction. Further, they are of a size that can be fabricated on a typical desktop MEX printer. Machines of this size – both single- and multi-material capable – are becoming increasingly common (Vaezi *et al.* 2013) in both hobbyist and industrial settings, with units such as the Ultimaker S3 and Prusa i3 meeting this specification (Ultimaker 2020; Prusa Research 2021). These machines typically use 0.4 mm nozzles, and this was presumed throughout the development of the process. The products are presented with volumetric and mass properties in Figure 12. Their mass properties were found through the use of weighing scales, custom tooling to align axes and a trifilar suspension system (du Bois, Lieven & Adhikari 2009). The CoM of case study B (the electric hand drill) was offset in the y- and z-axes to represent investigation into the use of an alternative battery – thought a viable use case for the technology. The values presented were used in all cases. Model geometry was either modelled (case A) or taken from a structured light scan of the original product (cases B and C).

5.2. Conventional 3D printing

To evaluate the proposed method, a set of results were generated using a conventional 3D printing process. To do this, the products were assumed to have a 1.2 mm
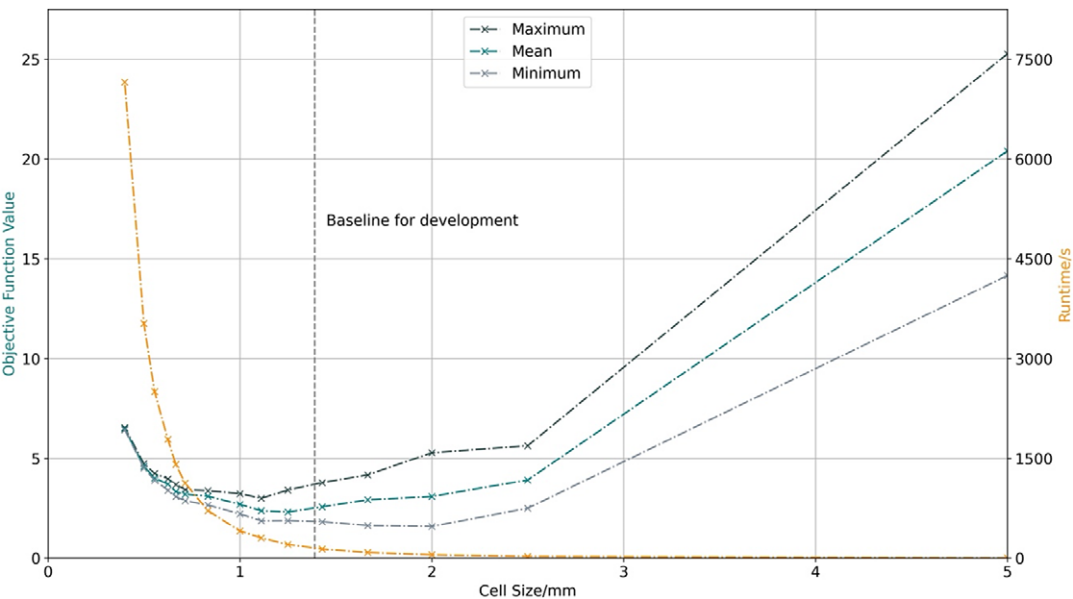

Figure 10. The effect of mesh density/cell size on objective function value and runtime.

Table 1. Objective function value and relative mass properties for each case (with respect to actual product properties) for conventional 3D printed fabrications and after emulation (marked*)

Case	Objective function value	Mass error (%)	Centre of mass position error			Rotational inertia error			Runtime/s	
			x (%)	y (%)	z (%)	xx (%)	yy (%)	zz (%)	Intel i5 9600	Apple M1
A	52.8	−49.6	−0.3	−2.7	0.3	−87.6	−38.0	−67.7		
B	92.9	−74.2	0.2	−3.7	14.2	−77.5	−77.6	−74.7		
C	65.4	−34.5	−1.2	5.7	24.0	−60.6	−63.9	−92.4		
A*	0.815	0.0	−0.1	−0.3	−0.4	−80.1	−15.4	−54.8	227.23	194.44
B*	2.487	−0.1	0.1	−1.2	1.1	−32.5	−30.6	−27.8	209.05	163.64
C*	28.943	−0.1	−1.0	6.1	21.8	−45.3	−49.9	−89.8	222.36	186.46

shell and 20% infill density (as per the default settings in Ultimaker Cura). The results from this work are presented in Table 1, with results for each mass property being given relative to the intended value. The CoM position errors are relative to the length (overall dimension) of the product in the respective axis. These are equivalent to the objective function terms (see equation 1).

5.3. Method setup

For the case studies, the parameters defined in Section 4 were used – specified at the end of the respective subsections. Cell sizes were determined for each case using the Ansys mech generator. The target value for mesh size was 45,000 giving 45,328, 44,999 and 45,447 for cases A to C, respectively.

5.4. Initial results

The results for the cases with meshes of ~45,000 cells are shown in Table 1, with results for each mass property being given relative to the intended value (results for the tuned process are indicated with an asterisk (*). The results demonstrate that the emulation process has been effective, reducing the objective function value for all products relative to the 20% infill PLA baseline in Table 1. Further, the error in mass property has only been increased for CoM position accuracy in x and z for Case A, and y for Case C, with these errors only increasing by 0.1%, 0.1% and 0.4%, respectively. Even the rotational inertia, terms (not considered by the objective function) were found to improve – with the average absolute error decreasing from 71.1% to 47.4% (averaged over the three cases and axes).

Case C demonstrates the lowest relative improvement in objective function value (55.7%), whilst case A exhibited the greatest relative improvement (98.5%). The two main reasons for the error observed in case C were related to the product's CoM position in the y- and z-axes, both of which required large deviations in the CoM from the GC. These mass distributions are shown in Figure 13.

The distribution for case C confirms the result from Table 1 and highlights that it is not possible to achieve the desired CoM position using the baseline process
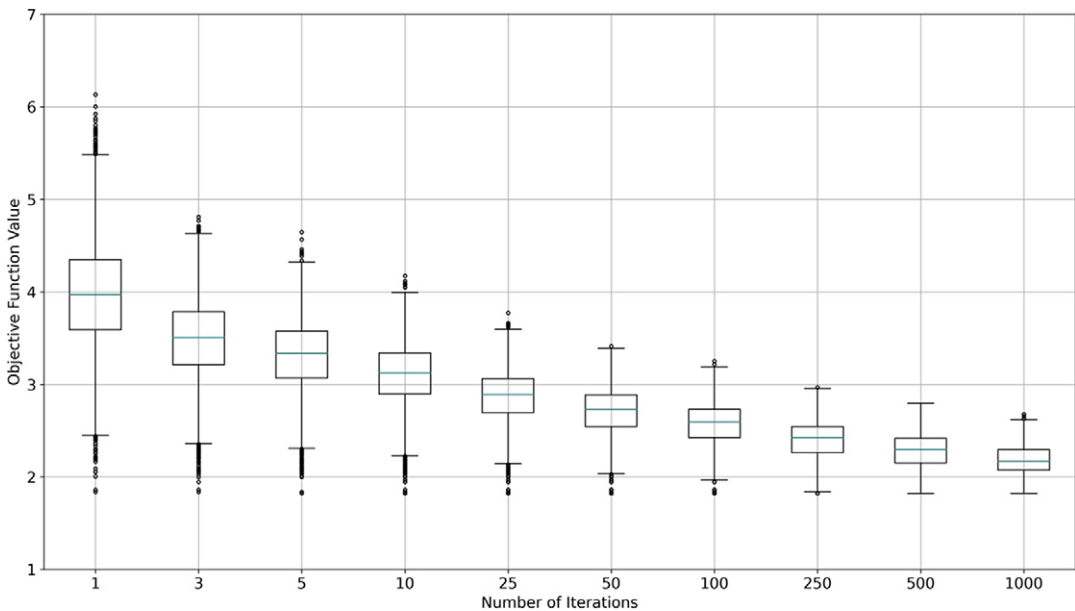
Figure 11. Effect of MCO iterations on objective function value. The box represents the interquartile range (IQR), with the inside line the median. The whiskers represent 1.5 times the IQR.

setup. This is because the targeted CoM position of the internal volume is found to be outside of the volume. Principally, this is due to the number of high-density cells required and the relative distance of the CoM from the GC. As such, the value of β is iterated to a result that flattens the exponential distribution across the product volume. This causes the probability of all cells being a high-density cell to be relatively consistent across the volume. Hence, when completing the MCO, the high-density cells are distributed evenly throughout the volume. It is likely that this issue would only occur in edge case products, such as case C, with limited movable mass and an intended CoM position relatively far from the GC.

To understand the context of these results, 20 blocks with 0, 20, 50 and 100% infill were printed using otherwise consistent print settings. It was found that the standard deviation for the mass of each of these blocks was ~1% of the respective block mean mass. As such, the numerical error from the emulation method is likely to be smaller than the as-printed error of the prototype (even with accurate machine-material calibration) due to inconsistency in deposition mass.

5.5. Sensitivity analysis

To understand whether the initial results could be improved for the three cases, a sensitivity analysis is performed to tune the emulation process. These include nozzle size, materials, β tolerance, cell size, internal volume searching limits and number of MCO iterations. These are presented in Sections 5.5.1 through 5.5.6 respectively.

5.5.1. Nozzle size

Nozzle size is directly related to the relative minimum cell density. Nozzle sizes of 0.1, 0.25, 0.4, 0.6 and 0.8 mm were investigated as these are common for desktop

MEX printers. Figure 14 presents the effect on each of the cases which all exhibit behaviour similar to the development case when the nozzle size (effectively the relative minimum cell density) is increased. The use of a smaller nozzle improves the emulation result, as expected.

If applications expect to use smaller nozzles for the purposes of improving the emulation result, it is important to consider the effect on print time and reliability, with previous examples discussed in literature (Felton, Hughes & Diaz-Gaxiola 2021). Reliability reduces also when using smaller nozzles due to nozzle blockages, whilst print time increases proportionally to the reduction in nozzle area – though this effect may be lessened if the volume of printed material is also decreased.

From this work, the use of a smaller nozzle provides an improved result. As such, the tuned results in Section 5.6 used a nozzle size of 0.1 mm for all cases.

5.5.2. Materials

Although PLA and copper-infused PLA have been used thus far, there are alternative materials available that offer a variety of material densities. Further, it is likely that the range will continue to increase as desktop MEX printers start to be capable of printing with metal-based materials. This can be achieved using materials such as BASF's Ultrafuse 316 L stainless steel metal-polymer (which has a printed part material density of 4.99 g/cm^3 (BASF 2019)). Normally, the use of this material requires debinding and sintering to form a solid stainless steel part; however, in this instance it is used in its *green* state to achieve higher printed material densities only (relative to other MEX printable materials). Testing was not undertaken to check that the Ultrafuse material could be printed with PLA, though it is expected that this should be possible. Future work should ensure that the secondary material can be printed with the base, primary material.

The values of the objective function are plotted for each of the case studies for a range of MDRs, in increments of 0.25, in Figure 15. It should be noted that it was not possible to achieve a result for Case B when using PLA alone as the mass could not be achieved (which resulted in a failed process).

Figure 13 presents and confirms that the use of PLA alone is a worse configuration than using a higher-density secondary material. Each of the cases displays similar behaviour to the development case, with the objective function result decreasing with increasing MDR, whilst the variability increases. It should be noted, however, that the variability for cases B and C was relatively small in comparison to case A. This was thought likely to be due to the greater volume and probability distribution applied to the product.

When tuning the process to achieve the best result, a MDR of 9 was used. To overcome the increased process variability, the number of MCO iterations was increased, and is discussed in Section 4.5.6. The ratio was limited to 9, corresponding to the ratio of the material density of lead to PLA.

5.5.3. β tolerance

The impact of β tolerances is presented in Figure 16. As discussed in Section 4.1.2, the use of a continuous probability distribution and a discrete mesh causes large increases in objective function values over small changes in β. This can be observed in the data for case A. As such, finely tuning β is not a deterministic process, and requires the use of a small value to ensure consistency. For this reason, the tuned
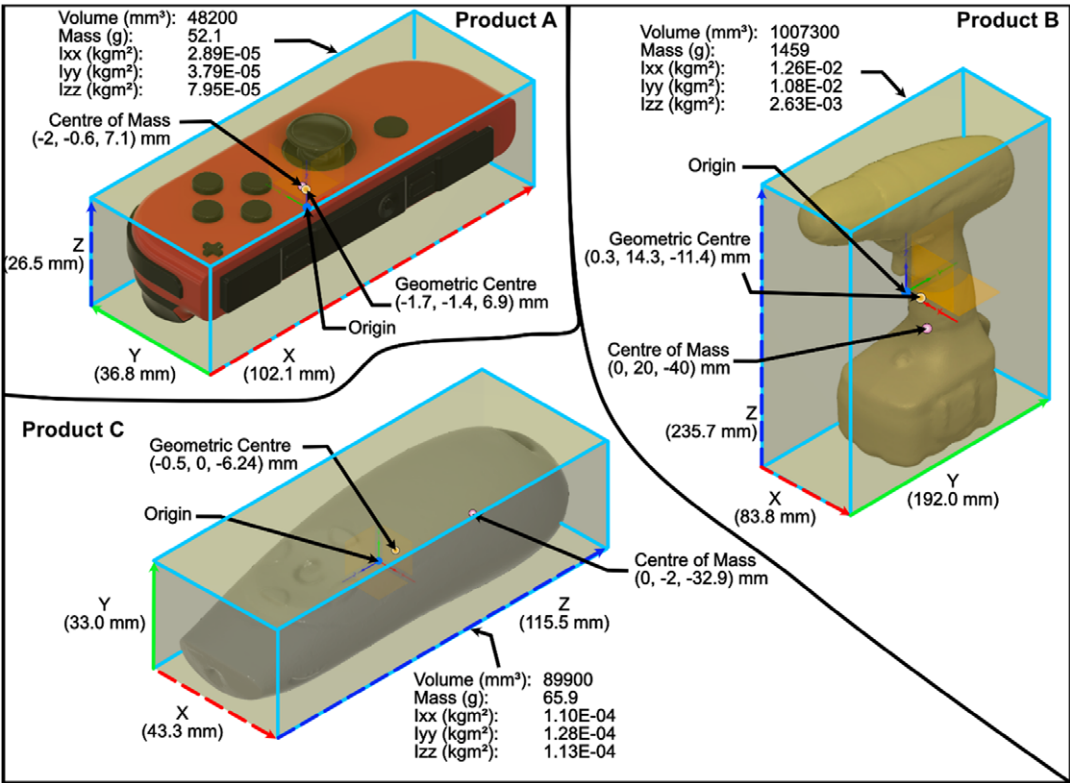
Figure 12. The three prototypical products considered within this work. Case A – a Nintendo Switch JoyCon, Case B – Bosch electric hand drill and Case C – laser pointer.
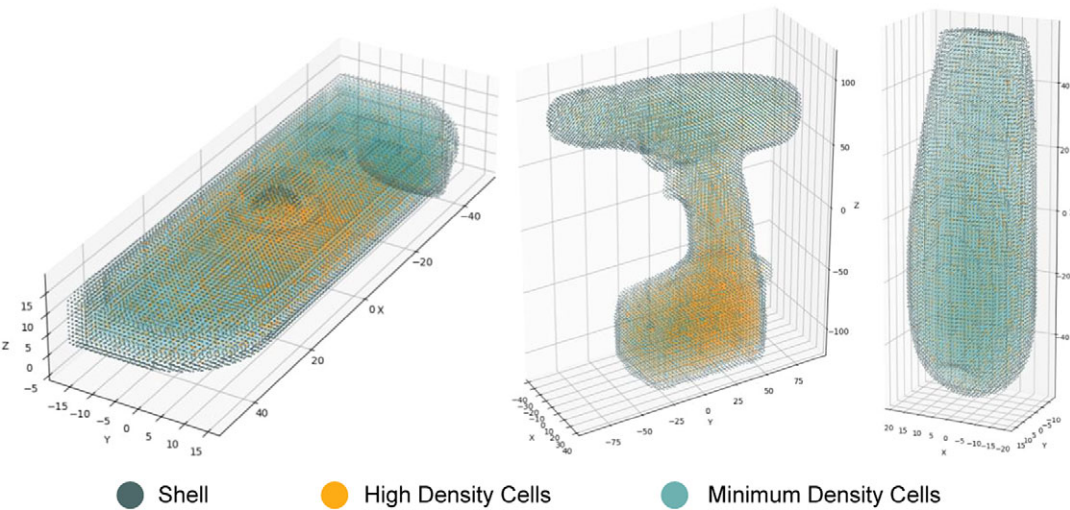
Figure 13. Example results for products (left-to-right) A, B and C showing the location of the shell, minimum-density cells and high-density cells.
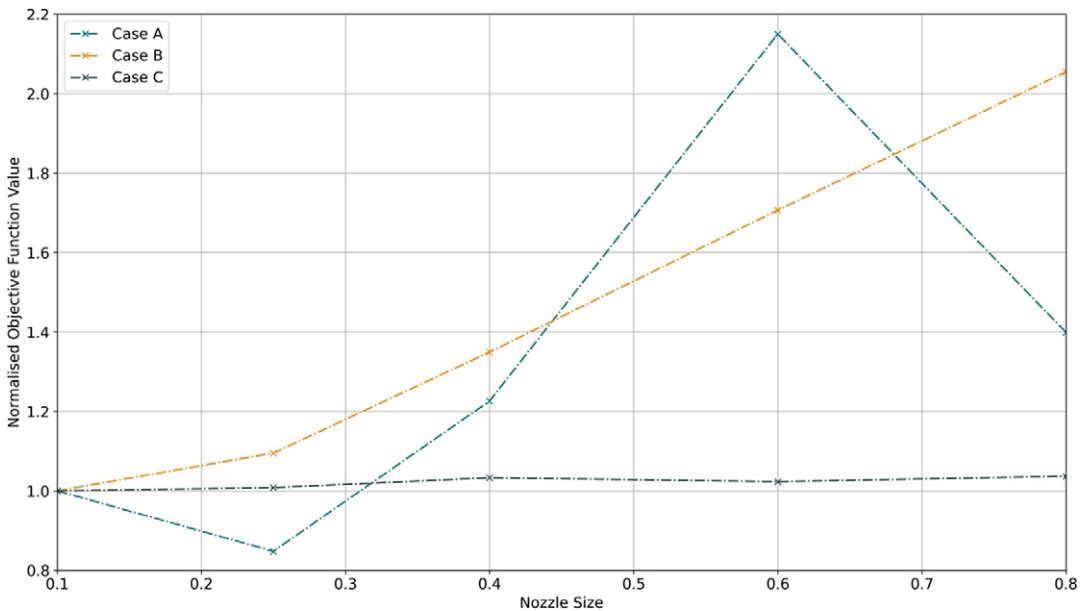
Figure 14. Normalised (to first data point of each case) objective function value for the three products when considering various nozzle sizes.

process used a β tolerance of 1. This meant that the number of high-density cells had to be within a single cell of the target.

5.5.4. Cell size

Meshes were generated with target cell sizes between 1 and 3 mm using Ansys for each case. Due to meshing errors, however, the actual mean cell size deviated from this target. The results for these meshes are presented in Figure 17, using the actual mean cell size for the x-position. Meshes for case B were not able to be generated with cell sizes less than 1.25 mm due to memory limitations. Meshing errors were also reported for Case A – at a targeted 1.5 mm – and B – at a targeted 2 mm – and so these meshes were excluded from the results.

For the three cases, the objective function value increased with cell size, at least for cell sizes above 1.5 mm, as was seen in the process development. Below cell sizes of 1.5 mm the relationship is less consistent, with this thought to be driven by the increasing relative minimum cell density. The exception to this is case C. Although this may be due to the ability of the process to place high-density cells more favourably, it was thought this improvement was likely to be due to every cell having a larger mass. This would mean that a reduced volume of high-density cells was necessary to achieve the target mass properties, allowing the exponential function to prioritise local cells more accurately (the shape parameter could increase). As such, the CoM error – particularly in the z-axis – could be reduced.

For the tuned process analysis, meshes with cell sizes of ~1.25 mm, ~1.5 mm and ~ 0.6 mm were used throughout.

22/34
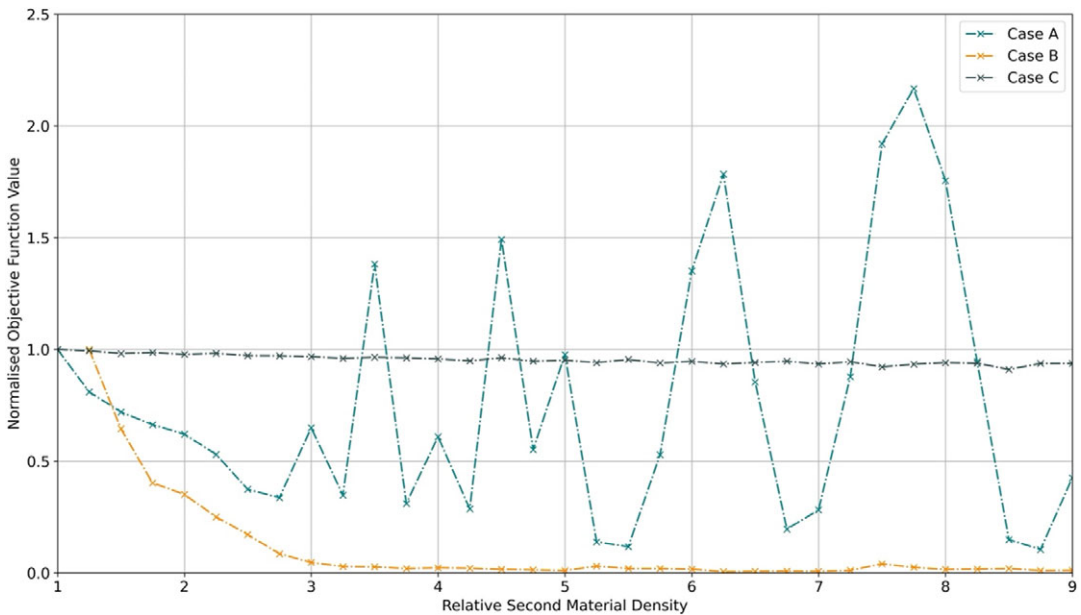
Figure 15. Normalised (to first data point of each case) objective function value for the three products when considering various secondary material configurations, presented using second material density relative to the PLA baseline. Case B's required mass could not be achieved when using PLA alone, which led to a process error, and is therefore not plotted here.

5.5.5. Internal volume centre of mass searching

Objective function values are plotted for a range of CoM iteration limits for each case in Figure 18. Case A has a very similar relationship as was discussed in Section 4.1.1, with objective function value decreasing with increasing CoM iterations. As such, there is not likely to be an optimum number of CoM iterations, with the error converging to a minimum. However, for the purposes of the tuned process, a value of 20 will be used, as the result appears to have started to converge.

Case B was able to initially improve the objective function result when increasing the number of CoM iterations – up to a limit of ~6 iterations. From here on the objective function value increases. A similar effect is seen in the results for case C, though this is from the offset with no CoM iterations improving on the initial result. Both effects are caused by the difficulty in localising sufficient mass around the target CoM position when the target CoM is external to the swept volume.

For the purposes of tuning the emulation process, CoM iteration limits of 20, 6 and 0 have been used for products A, B and C, respectively.

5.5.6. Monte Carlo optimisation

Finally, the number of iterations completed in the MCO process was considered. Previously, it was shown that increasing the number of MCO iterations generally improved the result and variability therein. To explore this further, 1,000 iterations were undertaken for each case and are shown in Figure 19.

As was expected, the accuracy improved and converged to a non-zero value when using a larger number of MCO iterations. After 1,000 iterations, the errors were 0.645, 2.28 and 28.65 for cases A, B and C, respectively. Of note was that case C

23/34
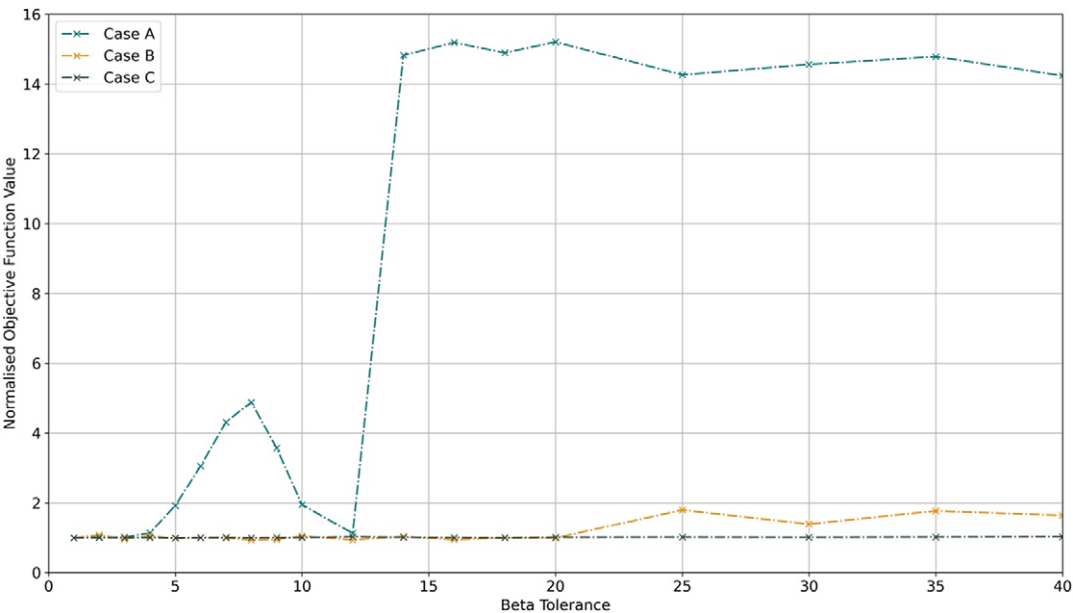
Figure 16. Normalised (to first data point of each case) objective function value for the three products when considering various β tolerances.
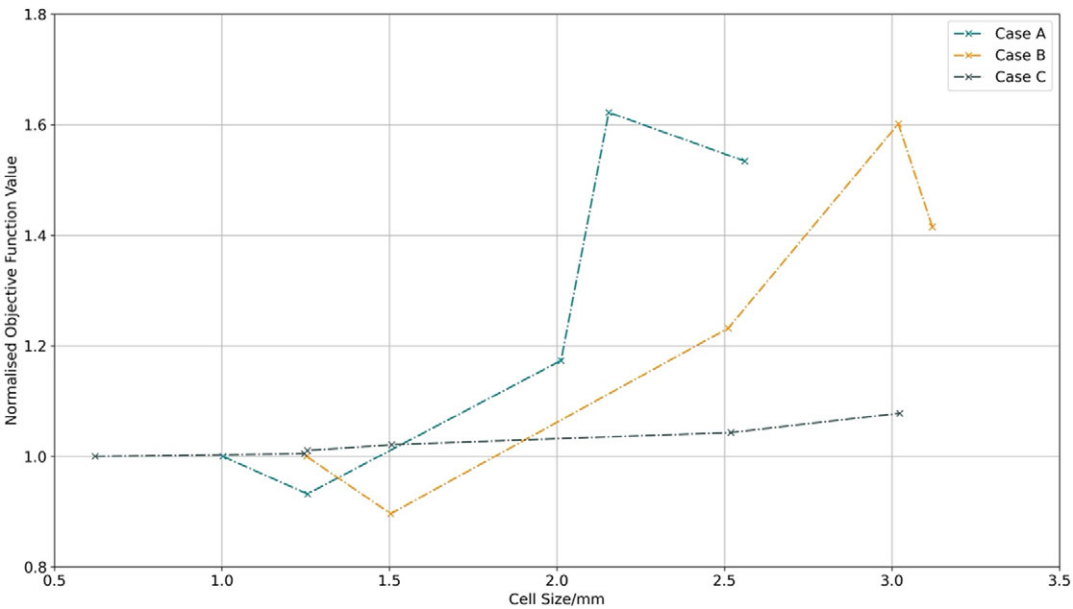
Figure 17. Normalised (to first data point of each case) objective function value for the three products for various cell sizes. Issues arose when meshing case B with cell sizes of 2 mm due to imperfect geometry – generated from a laser scan of the product – and less than 1.25 mm due to memory limitations.
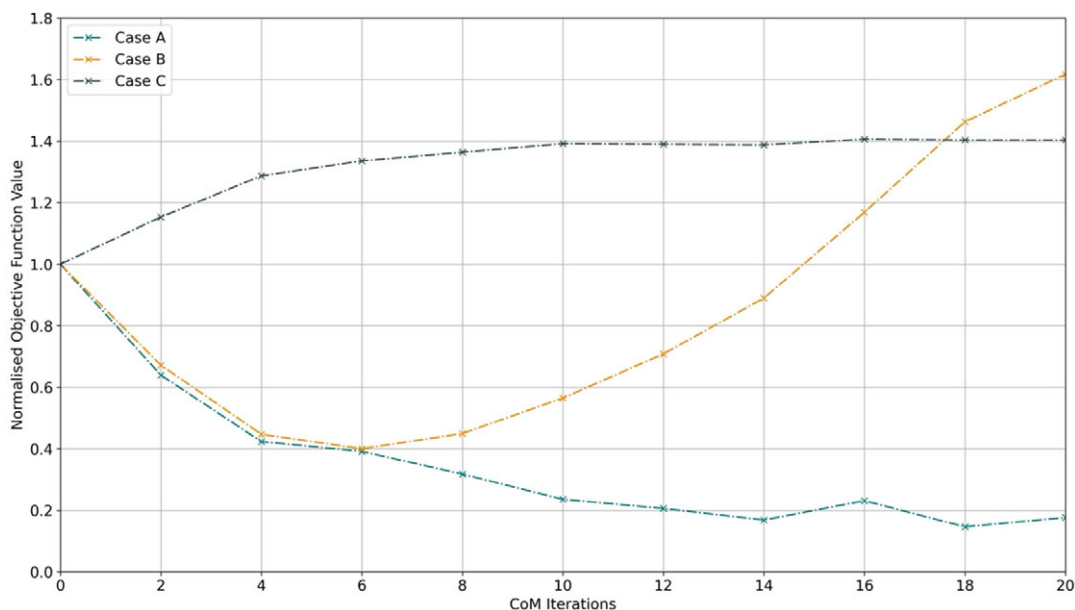
Figure 18. Normalised (to first data point of each case) objective function value for the three products for various CoM iterations.

showed little improvement with increasing MCO iterations. This reaffirms the notion that the exponential distribution was flattened across the product volume, leading to consistent results.

For the purposes of tuning the process to demonstrate a best-case result, 1,000 iterations will be used. Additional iterations may improve the result further, but all products showed signs of convergence when at 1,000 iterations, and, as such, any further improvement would likely be small.

5.6. Tuned results

Using the settings in the previous sections, a set of tuned results were generated for the three cases. However, it was recognised that there was cross-coupling between parameters that has not been fully investigated within this work. As such, there may still be scope for the results to improve further. For reference, the updated process parameters are shown in Table 2 for each product.

The tuned results in Table 3 demonstrate a significant improvement over the initial results, with improvements of 70.45%, 85.07% and 64.11% for cases A, B and C, respectively. This meant that the largest error in the considered mass properties, still the error in z-axis CoM position for case C, was reduced to 5.5% – equivalent to 6.35 mm.

The runtime was increased for each case, from an average of ~3 minutes to ~25.6 minutes. It is up to any potential user to decide if the extra computing time is warranted. It should be noted that although the relative increase in performance is large, the absolute improvement often relates to fractions of a gram and/or millimetres. Further, the fabrication time and cost would increase significantly
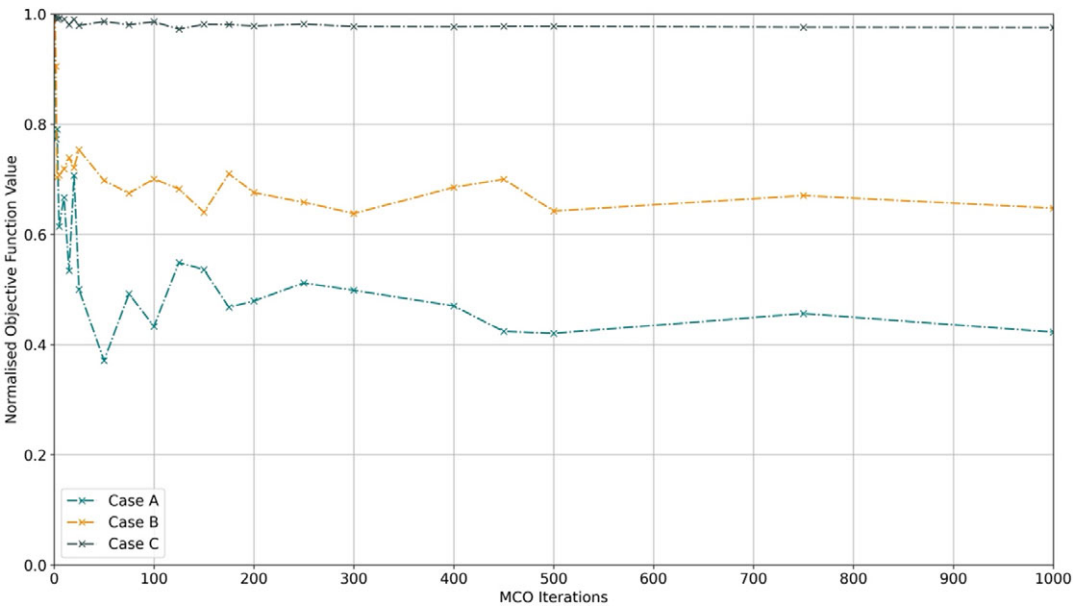
Figure 19. Normalised (to first data point of each case) objective function value for the three products for various MCO iterations.

Table 2. Tuned parameter settings

	Parameter					
Product	Nozzle size/ mm	Relative secondary material density	Cell size/ mm	β tolerance	CoM iterations	MCO iterations
A	0.1	9	~1.25	1	20	1,000
B	0.1	9	~1.5	1	6	1,000
C	0.1	9	~0.6	1	0	1,000

MCO, Monte Carlo optimisation.

Table 3. Tuned process results for the three prototypical products, relative to the desired mass properties for a nominal MEX fabrication

			Centre of mass position			Rotational inertia			
Product	Objective function value	Mass (%)	x (%)	y (%)	z (%)	xx (%)	yy (%)	zz (%)	Runtime/s (Apple M1)
A	0.24	0.1	−0.1	−0.1	0.0	−81.9	−37.2	−65.9	239.28
B	0.37	−0.2	−0.1	0.1	0.0	−58.4	−57.3%	−46.6	2208.73
C	10.39	0.0	−0.2	4.6	5.5	−61.0	−64.5	−91.8	2164.85

using the tuned parameters. As such, the parameters used for the initial results may be sufficient for real-world applications.

6. Discussion

The work detailed within this article has demonstrated that the use of a variable infill composition in MEX fabricated products could allow a product's relevant mass properties to be computationally emulated to high accuracy. In the best case presented here, this is to within 0.05 g and an average of ~0.03 mm in each axis. This work has, however, raised several interesting points for discussion. Within this section, these are explored, with the topics categorised as either physical, numerical or other considerations for clarity. In real-world applications there will be significant cross-correlation of parameters (both physical, numerical, and otherwise), and thus they should be considered together. Notably, as with the rest of this article, this section will focus on the computational emulation of mass properties in prototypes (the focus of this work) and how, in future work, what these results may mean for physical emulation.

6.1. Physical

It is asserted that the proposed process will increase print time. This is due to the volume of deposited filament likely to increase, and the discretisation of deposition slowing the process down. One potential advantage of using a higher-density secondary material would be to reduce this effect, with a smaller volume of material needing to be deposited. Currently, the main options are copper- or brass-infused PLA, as was used in this work, or stainless steel–infused PLA. Future work may investigate this further, including the development of alternative materials.

It is acknowledged that the accuracy of results achievable within this work is theoretical. To overcome this, further work should be undertaken that aims to fabricate products that have used this emulation methodology. Published work has also identified that the fabrication accuracy of the MEX process is likely to lead to greater errors than expected within the computational emulation process (Felton 2022). Further work should build upon this, identifying whether calibration steps can improve the physical emulation and, through doing so, identify the accuracy required from the computational workflow. Previous literature has shown that the geometric variability in the MEX process is often of the order of μm (Galantucci *et al.* 2015; Akbaş *et al.* 2019). Other work has investigated how process settings impact the deposited mass, with standard errors of ~0.32% (Afonso *et al.* 2021). As such, it should be possible to improve upon the published results, though some error will remain.

Additionally, work may identify the required accuracy to provide psychological benefit to stakeholders. This may follow similar methods to that presented in literature focussing on aesthetic quality (a common issue with 3D printed components). These methods range from quantification of qualitative measures (Galati & Minetola 2020) to automated measurement (Okarma *et al.* 2020). Other methods combine questionnaires and automation (Borgianni, Maccioni & Basso 2019), though other work has indicated that there is no direct link between surface roughness and perception (Hartcher-O'Brien, Evers & Tempelman 2019). However, the authors are unaware of any work looking directly at the psychological

impact of mass property emulation, and so this should be considered as a direct follow-up, with emphasis on identifying how quantitative measures correlate to perception.

This work has further assumed that the part is pre-oriented to the build direction, though this should not significantly affect the results if taken forward to manufacture in a different orientation aligned to an orthogonal axis. This is because the cells, although transformed through space, will need the same minimum infill structure, just oriented to a different axis. The main cause for error would be the layer height used no longer aligning to a unit cell size, though this error exists in the current form too (as the cells have some freedom to deviate from a predefined size in the meshing method). This error is expected to be small, though, with layer heights typically small (0.1–0.4 mm) and would likely average out over the part.

If the part were not oriented to one of the orthogonal axes (as currently defined), it is likely the part will need to be re-meshed and the mass distribution recalculated. This would be necessary to ensure that the minimum infill structure would adequately support all cells. The workflow should otherwise be identical.

6.2. Numerical

The use of a unit cell shell (single cell thickness) is one area that needs improvement in future iterations of the methodology. Although this assumption is appropriate when using cell sizes between 1 and 1.5 mm, the use of smaller cell sizes poses a risk to the successful fabrication of the product. This is because the shell may need to be comprised of a single deposition wall thickness, which can cause complications regarding whole product support, will mean that any print abnormalities are visible and is generally inadvisable. Conversely, the use of larger cell sizes and/or smaller nozzles may mean that the product shells are assumed to be larger than necessary. For example, the tuned parameters for case B assumed the use of a 0.1 mm nozzle with a 1.5 mm cell size. This would mean that the shell is formed of 15 layers, significantly more than common practice (3 or 4). As such, print time and cost are increased unnecessarily and the emulation result may be affected. It may be appropriate for future methods to use a separate shell mesh or use a variable mesh size.

To achieve the tuned results, several runs of the methodology with varying parameter values independently modified were required. It is likely, with the data presented within this work, that a future product would not require the same level of testing to identify the tuned parameters. However, some foundation product knowledge may be required (for example, relative CoM position from GC). As such, there is a time investment required to achieve this level of emulation accuracy outside of the runtime.

On the point of runtime, it should be recognised that the methodology developed herein uses a tool for the purposes of demonstration and has not been optimised. As such, time savings may be possible within the application/execution of the code, further reducing the effect on a user's pre-processing steps.

Case C demonstrated a limit of the methodology where the target CoM position falls outside of the product's swept volume, and the effectiveness of the probability distribution is diminished. This is actioned through the probability distribution being flattened across the product volume and thereby reducing the effect on the

resultant CoM position. To overcome this, it may be possible to apply a limit on the target CoM position with respect to the extent of the product geometry. Future work may investigate this further. In the meantime, it should be recognised that the method is primarily applicable to parts that avoid slender sections and do not require CoM offsets that would push the target internal volume CoM outside of the internal envelope.

6.3. Other

The consideration of print time also lends itself to a discussion around the use of alternative methods for mass property emulation in MEX products. The use of particulates – such as iron filings, lead pellets or similar – could reduce fabrication times by placing material into volumes as needed. Furthermore, higher cell densities may be achievable as filament material density limitations can be overcome. In this work, methods to support the material would need to be explored – with greater z-axis support required – as would automated placement of the material in-process. Additionally, the increased variability of the process would need to be considered (as observed when the secondary material density ratio was increased). This would necessitate the use of a larger number of MCO iterations. Lumped, solid masses would offer a similar solution, but would require a more extensive modification to the current MEX fabrication machinery and process and suffer from similar process-related issues. Further, limitations may arise caused by the requirement to "lump" mass (centralise as singular masses) together.

Lastly, the presented methodology does not consider whether certain mass properties are more important. In practice, it may be that the relative importance of emulating each of the mass properties would differ depending upon the case considered. This in turn may enable a trade-off to be determined that improves the emulation results for the mass properties of interest. Other work has looked at this further, demonstrating that principal RI is less important due to the central limit theorem dominating the perceived RI effects (Felton 2022). However, it would be beneficial to understand the psychological impact of mass and balance further.

7. Conclusions and future work

The scientific contribution of this article is two-fold: the creation of a numerical method for emulating the as-designed mass properties of MEX products through control of infill composition and the characterisation of the capability of the method to emulate mass properties in MEX (3D printed) prototypes.

The method is based on a directed optimisation approach that utilises solution space knowledge to target the resultant infill composition (whilst considering DfAM factors). The method was initially developed using a study of a simple primitive, which resulted in a set of initial (default) parameters. These parameters were applied to three case study products (case A – laser pointer, case B – hand drill and case C – games controller). The results demonstrated that individual mass and CoM position properties could be emulated to within ~1% of the target in less than 5 minutes CPU time. This was achieved using standard computer hardware and the initial parameter set. Exceptions were observed for case C, associated with the

relative offset between GC and CoM position, which are discussed within this work.

The method was refined (tuned) via repeat application to the three cases, but with relaxation of physical and reasonable computational limitations – such as considering a wider range of materials and allowing the runtime to be extended. Using the tuned parameter sets it was found that mass and CoM emulation error of 0.2% could be achieved for cases A and B. Case C continued to experience issues with CoM emulation, though the error was reduced from 21.8% to 5.5% in the worst instance. However, the runtimes associated with these improvements were significantly greater, increasing for case B from ~4 minutes to ~37 minutes.

In addition to comparison with the "as-designed" mass properties, the initial and tuned results were compared with standard (20%) infill MEX prototypes. This showed clear improvement in results at all stages. For cases A and B, emulation accuracy – as defined by the objective function – improved by 98.5% and 97.3% (respectively) when using the initial parameter set relative to the conventional fabrications. These improved further to 99.4% and 99.6%, respectively, when the tuned parameter sets were used, relative to the conventional fabrication results. This relates to a maximum CoM positional error reduction of 33.4 to 0.2 mm for a product of length ~ 236 mm in the associated axis. As such, the method demonstrates significant improvement in mass property representation relative to conventional MEX fabrications. The use of the baseline or tuned parameter set is, however, up to any future user who may wish to adopt this methodology, and should be based upon the resource available, the design context and what level of accuracy is required. Other work has demonstrated that calibration and other manufacturing issues within the MEX process will likely cause greater disparities in mass property accuracy (Felton 2022). As such, it is likely the initial parameter set is reasonable for most work, without also undertaking additional steps to calibrate the computational emulation and manufacturing processes.

The reported study is performed numerically using material and process parameters of typical (current) MEX machines. Over the forthcoming years both materials and capability (e.g. nozzle size) will improve, and, as such, these results should be taken as indicative of what may be possible in the future, with further improvement likely.

The developed numerical method demonstrates the potential capability for designers to fabricate prototypes using AM that embody representative mass properties, thereby significantly improving the feel of these parts. This enables highly automated manufacture with little required expertise to produce a prototype at a higher fidelity – with respect to the mass property aspects of feel – than has previously been possible. Due to the ease of use and low cost of AM techniques, such mass-emulated prototypes can be produced and applied early in the design process, which can both improve quality and reduce the time of the design process, and ultimately enable more successful product development.

Conversely, it should be recognised that the fabrication of large, heavy parts in this manner may delay the design process for rapid programmes due to the significant increase in print time (in the instance of one case study, increase from 2 to 9 days). Such increases may also increase design fixation due to time investment, and increased economic investment, in prototype fabrication (Youmans 2011). The effects of this are reduced through the ease of use and highly autonomous nature of the AM process but are not avoided entirely. It is therefore

recommended that such prototypes are – as with all prototyping activities – only created when the need for them arises.

Similarly, prototyping activities during the early stages of design should first consider emulating mass properties with simple approximate methods – for example, inserting solid masses into pockets – if a lower level of accuracy is appropriate. This also presents an additional work stream, where the level of appropriate emulation accuracy is investigated to minimise resources in the fabrication of applicable prototypes. This was not investigated within this work due to the complexities of identifying the required accuracy for the wide range of use cases, products, and design contexts that designers regularly work towards.

For future work, the authors will develop the method such that it can be integrated into current slicing tools to fabricate artefacts with emulated mass properties. As part of this, parameters that affect the deposition mass will be investigated (for example, layer height, print speed, extrusion temperature (Afonso *et al.* 2021)). It is posited that negative effects can be overcome through machine-material calibration, but some further uncertainty will affect the results.

References

Afonso, J. A., *et al.* 2021 Influence of 3D printing process parameters on the mechanical properties and mass of PLA parts and predictive models. *Rapid Prototyping Journal* **27** (3), 487–495; doi:10.1108/RPJ-03-2020-0043.

Akbaş, O. E., **Hıra, O.**, **Hervan, S. Z.**, **Samankan, S.** & **Altınkaynak, A.** 2019 Dimensional accuracy of FDM-printed polymer parts. *Rapid Prototyping Journal* **26** (2), 288–298; doi:10.1108/RPJ-04-2019-0115.

BASF 2019 *TDS Ultrafuse 316L*, online document (downloadable on August 17th 2021) www.basf-3dps.com.

Bassoli, E., **Denti, L.**, **Gatto, A.**, **Spaletta, G.**, **Paderno, A.**, **Zini, N.**, **Parrilli, A.**, **Giardino, R.**, **Strusi, V.**, **Dallatana, D.**, **Mastrogiacomo, S.**, **Zamparelli, A.**, **Iafisco, M.** & **Toni, R.** 2012 A combined additive layer manufacturing/indirect replication method to prototype 3D vascular-like structures of soft tissue and endocrine organs. *Virtual and Physical Prototyping* **7** (1), 3–11; doi:10.1080/17452759.2012.668701.

Borgianni, Y., **Maccioni, L.** & **Basso, D.** 2019 Exploratory study on the perception of additively manufactured end-use products with specific questionnaires and eye-tracking. *International Journal on Interactive Design and Manufacturing* **13** (2), 743–759; doi:10.1007/s12008-019-00563-w.

Buchenau, M. & **Suri, J. F.** 2000 Experience prototyping. In *Proceedings of the Conference on Designing Interactive Systems Processes, Practices, Methods, and Techniques - DIS '00*, pp. 424–433. ACM Press; doi:10.1145/347642.347802.

Camburn, B., **Viswanathan, V.**, **Linsey, J.**, **Anderson, D.**, **Jensen, D.**, **Crawford, R.**, **Otto, K.** & **Wood, K.** 2017 Design prototyping methods: state of the art in strategies, techniques, and guidelines. *Design Science* **3**, e13; doi:10.1017/dsj.2017.10.

Cross, R. & **Bower, R.** 2006 Effects of swing-weight on swing speed and racket power. *Journal of Sports Sciences* **24** (1), 23–30; doi:10.1080/02640410500127876.

Deininger, M., **Daly, S. R.**, **Sienko, K. H.**, **Lee, J. C.** & **Kaufmann, E. E.** 2019 Investigating prototyping approaches of Ghanaian novice designers. *Design Science* **5**, e6; doi:10.1017/dsj.2019.5.

Donati, C. & **Vignoli, M.** 2015 How tangible is your prototype? Designing the user and expert interaction. *International Journal on Interactive Design and Manufacturing* **9**, 107–114; 10.1007/S12008-014-0232-5.

du Bois, J. L., **Lieven, N. A. J.** & **Adhikari, S.** 2009 Error analysis in trifilar inertia measurements. *Experimental Mechanics* **49** (4), 533–540; doi:10.1007/s11340-008-9142-4.

Felton, H. 2022 *Improving User-Interaction with Material Extrusion Prototypes Through Emulation of Mass Properties. University of Bristol, Thesis*, online document. https://hdl.handle.net/1983/36aefdad-67dd-4962-ad6c-c94e5e9c2a9d.

Felton, H., **Hughes, R.** & **Diaz-Gaxiola, A.** 2021 Negligible-cost microfluidic device fabrication using 3D-printed interconnecting channel scaffolds. *PLOS One* **16** (2), e0245206; doi:10.1371/journal.pone.0245206.

Felton, H., **Yon, J.** & **Hicks, B.** 2020 Looks like but does it feel like? Investigating the influence of mass properties on user perceptions of rapid prototypes. In *Proceedings of the Design Society: DESIGN Conference* (*vol.* **1**), pp. 1425–1434. Cambridge University Press; doi:10.1017/dsd.2020.111.

Galantucci, L. M., **Bodi, I.**, **Kacani, J.** & **Lavecchia, F.** 2015 Analysis of dimensional performance for a 3D open-source printer based on fused deposition modeling technique. *Procedia CIRP* **28**, 82–87; doi:10.1016/J.PROCIR.2015.04.014.

Galati, M. & **Minetola, P.** 2020 On the measure of the aesthetic quality of 3D printed plastic parts. *International Journal on Interactive Design and Manufacturing (IJIDeM)* **14** (2), 381–392; doi:10.1007/s12008-019-00627-x.

Gibson, I., **Gao, Z.** & **Campbell, I.** 2004 A comparative study of virtual prototyping and physical prototyping. *International Journal of Manufacturing Technology and Management* **6** (6), 503–522; doi:10.1504/IJMTM.2004.005931.

Goudswaard, M., **Hicks, B.** & **Nassehi, A.** 2020 Towards the democratisation of design: a generalised capability model for FDM. *International Journal of Agile Systems and Management* **13** (1), 79–101; doi: 10.3233/978-1-61499-898-3-125.

Goudswaard, M., *et al.* 2022 Virtually hosted hackathons for design research: lessons learned from the international design engineering annual (IDEA) challenge 2021. In *Proceedings of the Design Society* (*Vol. 2*) pp. 21–30. Cambridge University Press; doi: 10.1017/pds.2022.3.

Hallgrimsson, B. 2012 *Prototyping and Modelmaking for Product Design*. Laurence King Publishing.

Hamon, C. L., **Green, M. G.**, **Dunlap, B.**, **Camburn, B. A.**, **Crawford, R. H.** & **Jensen, D. D.** 2014 Virtual or physical prototypes? Development and testing of a prototyping planning tool. In *Paper Presented at 2014 ASEE Annual Conference & Exposition*, Indianapolis, Indiana; doi:10.18260/1-2–23294.

Harris, C. R., **Millman, K. J.**, **van der Walt, S. J.**, **Gommers, R.**, **Virtanen, P.**, **Cournapeau, D.**, **Wieser, E.**, **Taylor, J.**, **Berg, S.**, **Smith, N. J.**, **Kern, R.**, **Picus, M.**, **Hoyer, S.**, **van Kerkwijk, M. H.**, **Brett, M.**, **Haldane, A.**, **Del Río, J. F.**, **Wiebe, M.**, **Peterson, P.**, **Gérard-Marchant, P.**, **Sheppard, K.**, **Reddy, T.**, **Weckesser, W.**, **Abbasi, H.**, **Gohlke, C.** & **Oliphant, T. E.** 2020 Array programming with NumPy. *Nature* **585** (7825), 357–362; doi:10.1038/s41586-020-2649-2.

Hartcher-O'Brien, J., **Evers, J.** & **Tempelman, E.** 2019 Surface roughness of 3D printed materials: comparing physical measurements and human perception. *Materials Today Communications* **19**, 300–305; doi:10.1016/j.mtcomm.2019.01.008.

Houde, S. & **Hill, C.** 1997 What do prototypes prototype? In *Handbook of Human-Computer Interaction*, pp. 367–381. Elsevier; doi:10.1016/b978-044481862-1.50082-0.

Lanzotti, A., **Grasso, M.**, **Staiano, G.** & **Martorelli, M.** 2015 The impact of process parameters on mechanical properties of parts fabricated in PLA with an open-source 3-D printer. *Rapid Prototyping Journal* **21** (5), 604–617; doi:10.1108/RPJ-09-2014-0135.

Lauff, C., **Kotys-Schwartz, D.** & **Rentschler, M. E.** 2017 Perceptions of prototypes: Pilot study comparing students and professionals. In *ASME 2017 International Design Engineering Technical Conferences and Computers and Information in Engineering Conference*. American Society of Mechanical Engineers Digital Collection; doi:10.1115/DETC2017-68117.

Luzanin, O., **Guduric, V.**, **Ristic, I.** & **Muhic, S.** 2017 Investigating impact of five build parameters on the maximum flexural force in FDM specimens - a definitive screening design approach. *Rapid Prototyping Journal* **23** (6), 1088–1098; doi:10.1108/RPJ-09-2015-0116.

Manoharan, V., **Chou, S. M.**, **Forrester, S.**, **Chai, G. B.** & **Kong, P. W.** 2013 Application of additive manufacturing techniques in sports footwear. *Virtual and Physical Prototyping* **8** (4), 249–252; doi:10.1080/17452759.2013.862958.

Mathias, D., **Ben, H.**, **Chris, S.** & **Charlie, R.** 2018 Characterising the affordances and limitations of common prototyping techniques to support the early stages of product development. In *Proceedings of International Design Conference* (*Vol.* **3**), pp. 1257–1268. Design Society; doi:10.21278/idc.2018.0445.

Mathias, D., **Snider, C.**, **Hicks, B.** & **Ranscombe, C.** 2019 Accelerating product prototyping through hybrid methods: coupling 3D printing and LEGO. *Design Studies* **62**, 68–99; doi:10.1016/j.destud.2019.04.003.

Melenka, G. W., **Schofield, J. S.**, **Dawson, M. R.** & **Carey, J. P.** 2015 Evaluation of dimensional accuracy and material properties of the MakerBot 3D desktop printer. *Rapid Prototyping Journal* **21** (5), 618–627; doi:10.1108/RPJ-09-2013-0093.

Mitchell, S. R., **Jones, R.** & **King, M.** 2000 Head speed vs. racket inertia in the tennis serve. *Sports Engineering* **3** (2), 99–110; doi:10.1046/j.1460-2687.2000.00051.x.

Nathan, A. M. 2003 Characterizing the performance of baseball bats. *American Journal of Physics* **71** (2), 134–143; doi:10.1119/1.1522699.

Okarma, K., **Fastowicz, J.**, **Lech, P.** & **Lukin, V.** 2020 Quality assessment of 3D printed surfaces using combined metrics based on mutual structural similarity approach correlated with subjective aesthetic evaluation. *Applied Sciences* **10** (18), 6248; doi:10.3390/app10186248.

Prusa Research 2021 Original PRUSA I3 MK35S+, online document (downloadable on May 12th 2021) https://shop.prusa3d.com/en/3d-printers/180-original-prusa-i3-mk3s-kit.html?gclid=CjwKCAjw-e2EBhAhEiwAJI5jgzl6xvBHh4hAwmkF0RZazJA89aGg9-jQ_4Mcxh7pO5lgTU_q9O9h7hoCl0YQAvD_BwE.

Python Software Foundation 2019 *Python 3.8 Reference Documentation*, online document (downloadable on April 23rd 2021) https://docs.python.org/3.8/.

RS Components 2021 *RS PRO 2.85mm Copper MT-COPPER 3D Printer Filament, 750g | RS Components*, online document (downloadable on June 21st 2021) https://uk.rs-online.com/web/p/3d-printing-materials/1254348/?cm_mmc=UK-PLA-DS3A-_-google-_-CSS_UK_EN_Computing_%26_Peripherals_Whoop-_-3D+Printing+Materials_Whoop-_-1254348&matchtype=&aud-842313741498:pla-304675461982&gclid=CjwKCAjw8cCGBhB6EiwAgORey9m9fO.

Sauer, J. & **Sonderegger, A.** 2009 The influence of prototype fidelity and aesthetics of design in usability tests: effects on user behaviour, subjective evaluation and emotion. *Applied Ergonomics* **40**, 670–677; doi:10.1016/j.apergo.2008.06.006.

Schmitt, M., **Mehta, R. M.** & **Kim, I. Y.** 2020 Additive manufacturing infill optimization for automotive 3D-printed ABS components. *Rapid Prototyping Journal* **26** (1), 89–99; doi:10.1108/RPJ-01-2019-0007.

Sculpteo 2021 *The State Printing of 3D Printing 2021, Sculpteo, p. 6.*

Ullman, D. 2010 *The Mechanical Design Process*, pp. 47–142. McGraw-Hill Education.

Ulrich, K. T. & **Eppinger, S. D.** 2016 *Product Design and Development.* McGraw-Hill.

Ultimaker 2020 *Ultimaker S3: Easy-To-Use 3D Printing Starts Here*, online document (downloadable on May 12th 2021) https://ultimaker.com/3d-printers/ultimaker-s3.

Vaezi, M., **Chianrabutra, S.**, **Mellor, B.** & **Yang, S.** 2013 Multiple material additive manufacturing – part 1: a review. *Virtual and Physical Prototyping* **8** (1), 19–50; doi: 10.1080/17452759.2013.778175.

Villacres, J., **Nobes, D.** & **Ayranci, C.** 2018 Additive manufacturing of shape memory polymers: effects of print orientation and infill percentage on mechanical properties. *Rapid Prototyping Journal* **24** (4), 744–751; doi:10.1108/RPJ-03-2017-0043.

Virtanen, P., **Gommers, R.**, **Oliphant, T. E.**, **Haberland, M.**, **Reddy, T.**, **Cournapeau, D.**, **Burovski, E.**, **Peterson, P.**, **Weckesser, W.**, **Bright, J.**, **van der Walt, S. J.**, **Brett, M.**, **Wilson, J.**, **Millman, K. J.**, **Mayorov, N.**, **Nelson, A. R. J.**, **Jones, E.**, **Kern, R.**, **Larson, E.**, **Carey, C. J.**, **Polat, İ.**, **Feng, Y.**, **Moore, E. W.**, **VanderPlas, J.**, **Laxalde, D.**, **Perktold, J.**, **Cimrman, R.**, **Henriksen, I.**, **Quintero, E. A.**, **Harris, C. R.**, **Archibald, A. M.**, **Ribeiro, A. H.**, **Pedregosa, F.**, **van Mulbregt, P.** & **SciPy 1.0 Contributors**. 2020 SciPy 1.0: fundamental algorithms for scientific computing in python. *Nature Methods* **17** (3), 261–272; doi:10.1038/s41592-019-0686-2.

Wiethoff, A., **Schneider, H.**, **Küfner, J.**, **Rohs, M.**, **Butz, A.** & **Greenberg, S.** 2013 Paperbox: a toolkit for exploring tangible interaction on interactive surfaces. In *Proceedings of the 9th ACM Conference on Creativity & Cognition*. Association for Computing Machinery, pp. 64–73; doi:10.1145/2466627.2466635.

Youmans, R. J. 2011 The effects of physical prototyping and group work on the reduction of design fixation. *Design Studies* **32** (2), 115–138; doi:10.1016/j.destud.2010.08.001.